Journal of ELECTRONIC MATERIALS, Vol. 50, No. 4, 2021
https://doi.org/10.1007/s11664-021-08777-z

REVIEW ARTICLE

Room Temperature Ferromagnetism: Nonmagnetic Semiconductor Oxides and Nonmagnetic Dopants

SAAD MABROUK YAKOUT [1,2,3]

1.—Inorganic Chemistry Department, National Research Centre (NRC), El Buhouth St., Dokki, Cairo 12622, Egypt. 2.—e-mail: s_mabrok2002@yahoo.com. 3.—e-mail: sm.yaqut@nrc.sci.eg

Advances in room temperature ferromagnetic semiconductors increase the opportunity to commercialize full spintronic devices. The manipulation of electron spin in semiconductor materials has driven significant research activity with the goal of realizing their amazing technological potential. Coupling of magnetic and semiconducting properties could lead to a new generation of information and communication devices. During the past 20 years, the intensive research on magnetic semiconductor materials has led to discovery of two interesting facts. Room temperature ferromagnetism is observed in undoped semiconductor oxides with empty or completely filled d- or f-orbitals, and nonmagnetic dopants can induce or enhance the room temperature ferromagnetism in nonmagnetic semiconductor materials. The organized review which addresses this phenomenon and covers the large number of studies on this subject is rare. In this study, we firstly review the advantages aspects of spintronic devices as well as the materials suitable for these applications. Here, we tried to provide a systematic study on defects induced by room temperature ferromagnetism in undoped semiconductor oxides as well as the impact of nonmagnetic dopants on ferromagnetism. We hope this review assist researchers in creating a complete picture to develop future research activities to access innovative technological applications.

Key words: Electronics, magnetic semiconductor, room temperature ferromagnetism, d^0 magnetism, nonmagnetic dopants, innovative spintronic devices

INTRODUCTION

Manipulation of electric charge in semiconductor materials and their heterostructures has led to the advent of electronic and optoelectronic devices.[1] Computers, TVs and smartphone devices are some of the great results of this technology.[2] The miniaturization of electronic components such as transistors and capacitors in integrated circuits is central to the modern electronic device boom.[3,4] A transistor and capacitor are paired together to create a memory cell, which represents a single bit of data.[5] The capacitor holds the bit of information as 0 (low voltage level) or 1 (high voltage level). The transistor acts as a switch that lets the control circuitry on the memory chip read the capacitor or change its state. Recently, this technology has faced some obstacles related to transistor node size, energy consumption and volatility of data.[4,6–8] Currently, the transistor node size reaches 5 nm with the highest transistor density of 171.3 million.[9,10] Atomic size is an insurmountable obstacle limit for transistor node minimization. In RAM, the capacitors must be re-charged continuously to retain data, which consume more energy.[8] Also, if the electronic device's power is cut off, the information stored in the RAM is lost.[8] Spintronics is new technology emerging to solve the problems existing in

(Received November 8, 2020; accepted January 21, 2021; published online February 20, 2021)

conventional electronic devices.[11,12] Spintronics is based on manipulation of electron spin instead of electric charge in bulk semiconductors to process and store information in a single chip,[13] as illustrated in Fig. 1.

In the twenty-first century, it is anticipated that the spin degree of freedom in semiconductors will play a crucial role in the development of information technologies.[1] This new technology requires semiconductor materials with special magnetic properties.[14,15] Combining information processing and storage in a single chip requires coupling of semiconducting and magnetic properties in a single material at room temperature.[14,15] Diluted magnetic oxide semiconductors are a special class of magnetic semiconductor materials which are strong candidates to satisfy the requirements for spintronic device fabrication.[16–18] The expected way to obtain these materials is to add magnetic ions (Mn, Fe, Co, Ni) to semiconductor materials. Indeed, in 2000, a big boost to the experimental efforts to realize room temperature ferromagnetic semiconductor was reported in a theoretical work provided by Dietl et al., in which they predicted room temperature ferromagnetism in Mn-doped ZnO and GaN.[19] This discovery led to a series of experimental efforts to confirm the possibility of inducing room temperature ferromagnetism in TiO_2 and ZnO via transition metal doping. Experimentally, in 2001 and 2002, real room temperature ferromagnetic behavior was reported in Co-doped TiO_2,[20] Co-doped ZnO,[21] V-doped ZnO,[22] Fe/Cu-codoped ZnO,[23] Co/Fe-codoped ZnO.[24] Later, these results lead to extensive research activities focusing on diluted magnetic oxide semiconductors (DMOSs), aiming to understand the mechanisms involved and to design better materials suitable for practical applications.[25–27] However, the major obstacle in magnetic ion-doped semiconductors is that the transition metal dopant can undergo a segregation to form magnetic-clusters or secondary phases. As a result, there is much debate about whether the observed room temperature ferromagnetism is an intrinsic or extrinsic property of the material. The magnetic clusters and secondary phases are big problems facing the practical applications which need stable ferromagnetic properties from an intrinsic single-phase structure.

Interesting results ruled out the role of magnetic secondary phases or impurities in magnetic clusters have emerged during work on these materials.[28–31] Room temperature ferromagnetism is observed in undoped nanostructured semiconductor oxides with d^0 or f^0 configuration and nonmagnetic dopants can induce room temperature ferromagnetism in nonmagnetic materials. These two interesting results

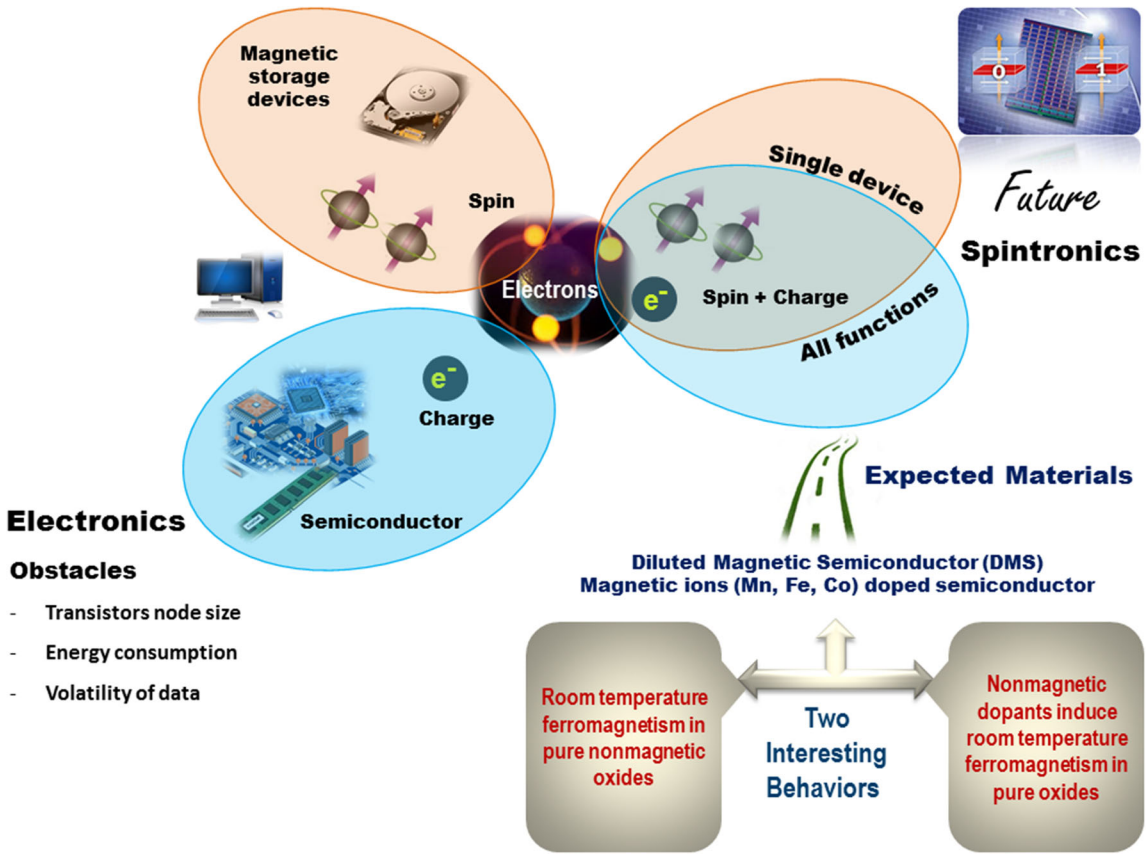

Fig. 1. Connected view demonstrating the basic concept of transfer from electronics to spintronics technologies.

completely eliminate the role of magnetic clusters or a secondary phase, which assists in realizing the practical applications. Many scientists work to realize strong room temperature ferromagnetism with suitable magnetic parameters in undoped semiconductor oxides or by means of using nonmagnetic dopants. Synthesis, site engineering by nonmagnetic dopants, annealing under different atmospheres, and thin film modifications represent the basic techniques in realizing strong room temperature ferromagnetism. Lately, two-dimensional (2D) materials also have been drawing tremendous attention in the spintronics field due to their unique spin-dependent properties such as the ultra-long spin relaxation time of graphene and the spin–valley locking of transition metal dichalcogenides.[32–34] Furthermore, the related heterostructures can provide an extraordinary probability of merging the different characteristics through a proximity effect, which could solve the limitation present in individual two-dimensional structures. Therefore, proximity engineering has been growing extremely fast and has made significant achievements in spin injection and manipulation.[32–34]

In this review we will focus on the room temperature ferromagnetism induced via defects or through using nonmagnetic dopants in semiconductor oxides. In the fundamentals sections, we present full representation to room temperature ferromagnetism in undoped semiconductor oxides with clear classification of nonmagnetic dopants used to induce or improve room temperature ferromagnetism in nonmagnetic oxides materials.

Non-Traditional Room Temperature Ferromagnetism

Traditionally, magnetism has a similar origin in all magnetic materials; it is defdined as the presence of localized electrons in the partially filled d- or f-orbitals of transition or rare earth elements, which have a corresponding localized spin or magnetic moment. The exchange interactions between the localized moments lead to magnetic order. It is expected that there is no magnetism in the presence of d^0 or f^0 configuration or through addition of a nonmagnetic dopant to a nonmagnetic material. This is not the truth; interestingly, nanostructures of undoped semiconductor oxides exhibit a room temperature ferromagnetic hysteresis loop, and nonmagnetic dopants have shown the ability to induce or enhance magnetic properties in nonmagnetic material.[28–31] The importance of room temperature ferromagnetic behavior in undoped semiconductor oxides, or due to nonmagnetic dopants, is the exclusion of the influence of ferromagnetic impurities which may be formed as a result of use of magnetic transition elements.

The experimental observations of these interesting results started in 2004 and 2005 and developed with time to include more undoped nanostructured materials and new families of nonmagnetic dopants.[35,36] Figure 2 demonstrates the classification of nonmagnetic materials and nonmagnetic dopants related to room temperature ferromagnetism; the tree shape symbolizes the continuous growth of these materials. Herein, two separate parts about these results were reviewed in detail with the aim of creating a comprehensive picture to help researchers access their technological applications.

Room Temperature Ferromagnetism: Undoped Semiconductor Oxides

The first mention of room temperature ferromagnetism in nonmagnetic undoped semiconductor oxides was reported on HfO_2 films by Venkatesan et al. in 2004.[35] These films exhibit room temperature ferromagnetism with measured Curie temperature exceeding 227°C and a magnetic moment of around 0.15 bohr magnetons per HfO_2 formula unit. The same group reported a more detailed study on films of different thicknesses, obtained by pulsed-laser deposition under different conditions and on different substrates.[37] For all these undoped films the Curie temperatures were found far beyond 400 K. However, it turns out that the value of the magnetic moment does not depend clearly on either the film thickness or the type of the substrate. Apparently, the moments are unstable over extended periods of time. Indeed, a decrease of about 10% of the moment is observed after 6 months.

In 2006, Hong et al. reported remarkable room temperature ferromagnetism in undoped TiO_2, HfO_2, and In_2O_3 thin films.[38] As mentioned by the authors, In_2O_3 thin films exhibit a modest magnetic moment when prepared on MgO substrates while those deposited on Al_2O_3 substrates have a negative diamagnetism. In contrast, TiO_2 and HfO_2 thick films (200 nm) showed large magnetic moments of 20 and 30 emu/cm^3, respectively. Since bulk TiO_2, HfO_2, and In_2O_3 are clearly diamagnetic, the authors attributed this behavior to defects or oxygen vacancies present in the thin film form of these oxides. Interestingly, in the same year, Sundaresan et al. stated that the ferromagnetism can be considered a universal phenomenon of nanoparticles of the otherwise nonmagnetic oxides.[28] In their study, CeO_2, Al_2O_3, ZnO, In_2O_3, and SnO_2 nanoparticles with diameters between 7 and 30 nm revealed room-temperature ferromagnetism. Furthermore, the saturated magnetic moments of CeO_2 and Al_2O_3 nanoparticles are comparable to those observed in transition metal-doped wide band semiconducting oxides. ZnO, In_2O_3, and SnO_2 nanoparticles show somewhat lower values of magnetization but with a clear hysteretic behavior. Conversely, the bulk samples obtained by sintering the nanoparticles at high temperatures in air or oxygen became diamagnetic. As there were no magnetic impurities present,

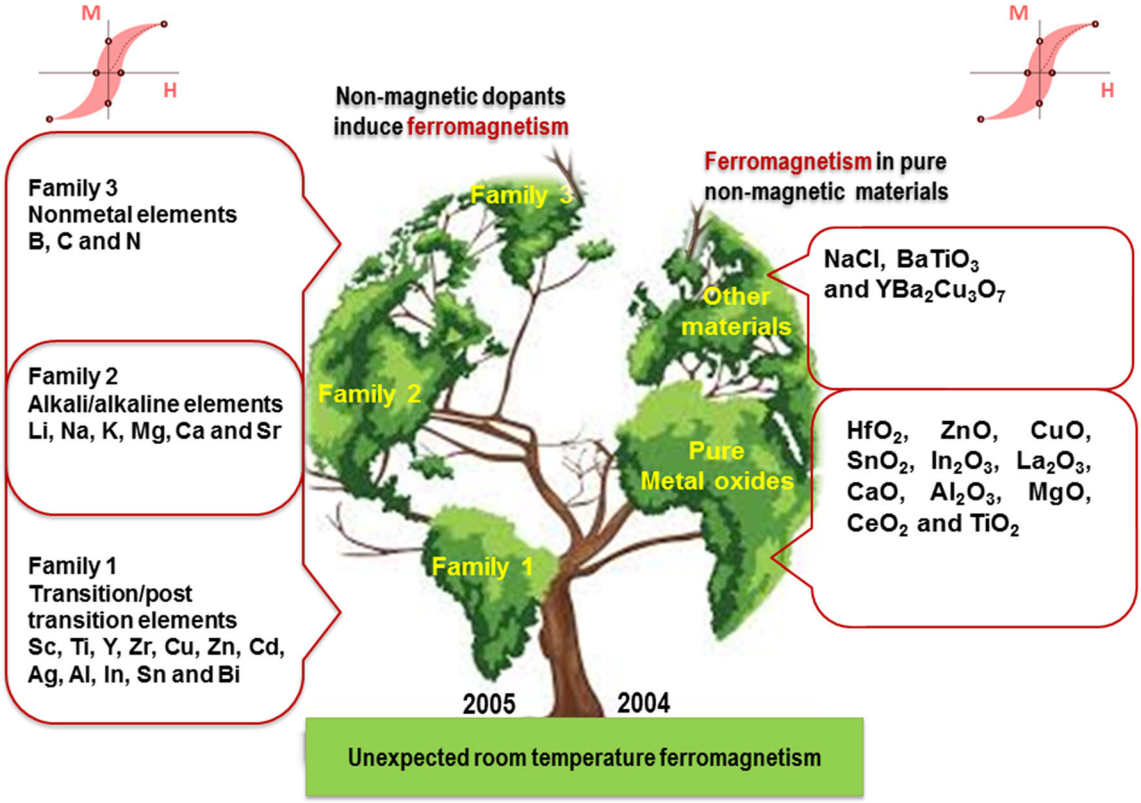

Fig. 2. Room temperature ferromagnetism in undoped nonmagnetic materials or due to nonmagnetic dopants; the tree symbolizes continuous growth.

the authors assume that the origin of ferromagnetism may be the exchange interactions between localized electron spin moments resulting from oxygen vacancies at the surfaces of nanoparticles. Based on these results they suggest that ferromagnetism may be a universal characteristic of nanoparticles of metal oxides. Later, in 2007, the numbers of studies which confirm the room temperature ferromagnetism in undoped semiconductors are increased. Xiao et al. published a scientific paper showing anomalous room temperature ferromagnetic behavior of CuO nanorods (30–40 nm in diameter and 100–200 nm in length) synthesized via a hydrothermal method as shown in Fig. 3.[39] The coercive force (Hc) of the synthesized CuO nanorods at T = 300 K was estimated to be 175.88 Oe.

Rumaiz et al. deposited pure TiO_2 films on Si substrates by pulsed laser deposition (PLD) to study the relation between defects and ferromagnetism.[40] Interestingly, they experimentally found room temperature ferromagnetism in these films with magnetic moment directly related to oxygen vacancy concentration. The magnetic properties of highly pure semiconducting anatase $TiO_{2-\delta}$ grown on (1 0 0) $LaAlO_3$ at different oxygen pressures have been investigated by Yoon et al.[41] They demonstrate that $TiO_{2-\delta}$ films exhibit ferromagnetism up to 880 K without the introduction of magnetic ions. In the

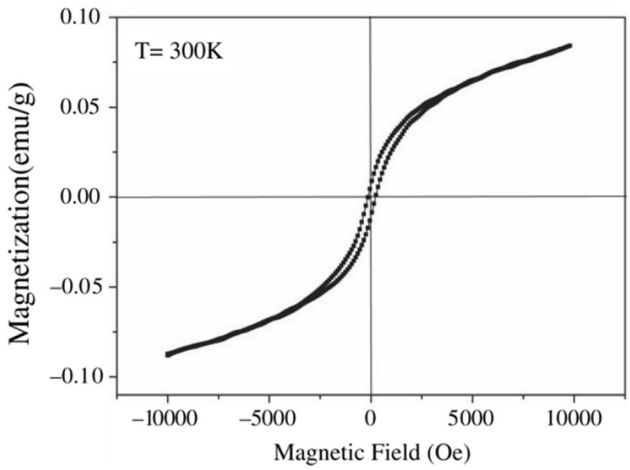

Fig. 3. Dependence of magnetization on the applied magnetic field for CuO nanorods. The figure is reprinted with permission from reference[39] under terms and conditions provided by Elsevier and Copyright Clearance Center. http://www.copyright.com/publishers/rightslink-permissions.

same context, Sanyal et al. studied the origin of room temperature ferromagnetism in nanocrystalline ZnO as well as the defect–magnetization correlation.[42] Remarkably, they observed that nanocrystalline ZnO chemically prepared by firing at 550°C showed room temperature ferromagnetic ordering with a saturation magnetization of 1.3×10^{-3} emu/gm. In contrast, bulk ZnO, ball milled

nanocrystalline ZnO and chemically prepared nanocrystalline ZnO samples without firing show diamagnetic and paramagnetic characteristics. Thus, depending upon the preparation method, the magnetic property of the nanocrystalline ZnO shows diamagnetic, paramagnetic and even ferromagnetic nature. The influence of vacuum and air annealing on room temperature ferromagnetism of TiO_2 thin films synthesized using both spin coating and sputter deposition on sapphire and quartz substrates were investigated by Sudakar et al.[43] As mentioned by the authors, all films annealed in vacuum exhibit room temperature ferromagnetic properties while those annealed in air display much smaller, often negligible, magnetic moments. They found that the magnetization and magnetization per unit area of these samples depends on film thickness and it decreases monotonically with increasing the thickness. Their results suggest that room temperature ferromagnetism of TiO_2 films annealed in vacuum is mediated by surface defects or interfacial effects, but does not arise from stoichiometric crystalline TiO_2. In the same way, Hassini et al. showed that the confinement effects is an important factor plus defects in inducing room temperature ferromagnetism in TiO_2 thin films prepared by spin coating.[44]

For the second time, Sundaresan and Rao mentioned in new study that the ferromagnetism is a universal feature of inorganic nanoparticles.[45] The authors noticed that the nanostructure form can cause the diamagnetic behavior of CeO_2, TiO_2, Al_2O_3, MgO, GaN, $BaTiO_3$ and superconducting $YBa_2Cu_3O_7$ to be ferromagnetic at room temperature compared to the bulk. As shown in Fig. 4 and based on their discussion, the ferromagnetism of the nanoparticles is confined to the surface effect, and the classical ferroelectric $BaTiO_3$ can show multiferroic properties at nano-scale. In another remarkable study, in 2013, Li et al. found strong room temperature ferromagnetism in undoped ZnO nanostructure arrays prepared by colloidal template as shown in Fig. 5.[46] High saturation magnetization of 6.1 emu g^{-1} and a remarkable dependence of ferromagnetism on grain size were reported in this work, as shown in Fig. 6. By adjusting the annealing time of the synthesized ZnO, the saturation magnetization can be varied from 0.1 to 6.1 emu g^{-1}. The authors clearly show that grain size and oxygen vacancies are the main factors for such ferromagnetism.

With respect to La_2O_3, Xu et al. detected room temperature ferromagnetism in pure La_2O_3 nanoparticles synthesized via precipitation and post-annealing method.[47] The magnetic hysteresis loop measurements show that all La_2O_3 samples exhibit room temperature ferromagnetism and the saturation magnetization was decreased from 0.0033 emu/g to 0.0018 emu/g due to increasing the annealing temperature from 700 to 1000 °C. In the case of CaO, the ferromagnetic hysteresis loop at room temperature was found in CaO nanopowders prepared by the sol-gel method.[48] Also, the authors found that the saturation magnetization decreases from 0.031 to 0.007 emu/g by increasing the annealing temperature from 700 to 1000 °C. Their experimental results and first principle calculations pointed out that Ca defects are the reason for the ferromagnetic behaviour in CaO nanopowders. The studies also confirmed that pure Y_2O_3 nanoparticles synthesized by a glycine-nitrate method have room temperature ferromagnetism.[49] Interestingly, they noticed that the vacuum-heated sample shows the largest ferromagnetism and also pressing the samples before heat treatment enhanced the saturation magnetization value. The Y_2O_3 nanoparticles exhibited the largest saturation magnetization value of 0.0282 emu g^{-1} when annealed in vacuum due to formation of numerous oxygen vacancies.

Surprisingly, NaCl (a nonmagnetic inorganic nonmetallic material) with different crystal size revealed room temperature ferromagnetism which provides a novel opportunity to further understand the origin of ferromagnetism in the traditional substances as illustrated in Fig. 7.[50] They noticed that the saturation magnetization (Ms) of NaCl increases monotonically from 8.66×10^{-5} emu/g to 1.08×10^{-3} emu/g due to a decrease of particle size. The authors suggest that the ferromagnetism in NaCl originates from a surface effect due to interactions between the surface Cl vacancies which form the long range ferromagnetic order. On the other hand, it was observed that mixing of pure nonmagnetic oxides in heterostructures or nanocomposites induces abnormal room temperature ferromagnetic behaviour with enhanced magnetic parameters.[51–53] In this context, Gao et al. found enhanced room temperature ferromagnetism in CuO–ZnO heterostructures compared to a single component, as shown in Fig. 8.[51] The maximum saturation magnetization (0.022 emu g^{-1}) was realized in the sample with molar ratios of ZnO:CuO = 33:67. They attributed the enhanced ferromagnetism to an interface effect which opens a new way to design magnetic materials for promising devices. More details about defect-induced room temperature ferromagnetism in undoped materials are included in Table I.

Room Temperature Ferromagnetism: Nonmagnetic Dopants

Nonmagnetic Transition Elements

Sc, Ti, Y, Zr, Cu, Zn, Cd and Ag are typical examples of nonmagnetic dopants that belong to transition metal elements. The first attempt to use nonmagnetic dopants in inducing room temperature ferromagnetism was related to copper, which is considered an important step in this field.[36] Copper, Cu, is thought to be an ideal nonmagnetic dopant for undoped metal oxides, because the secondary

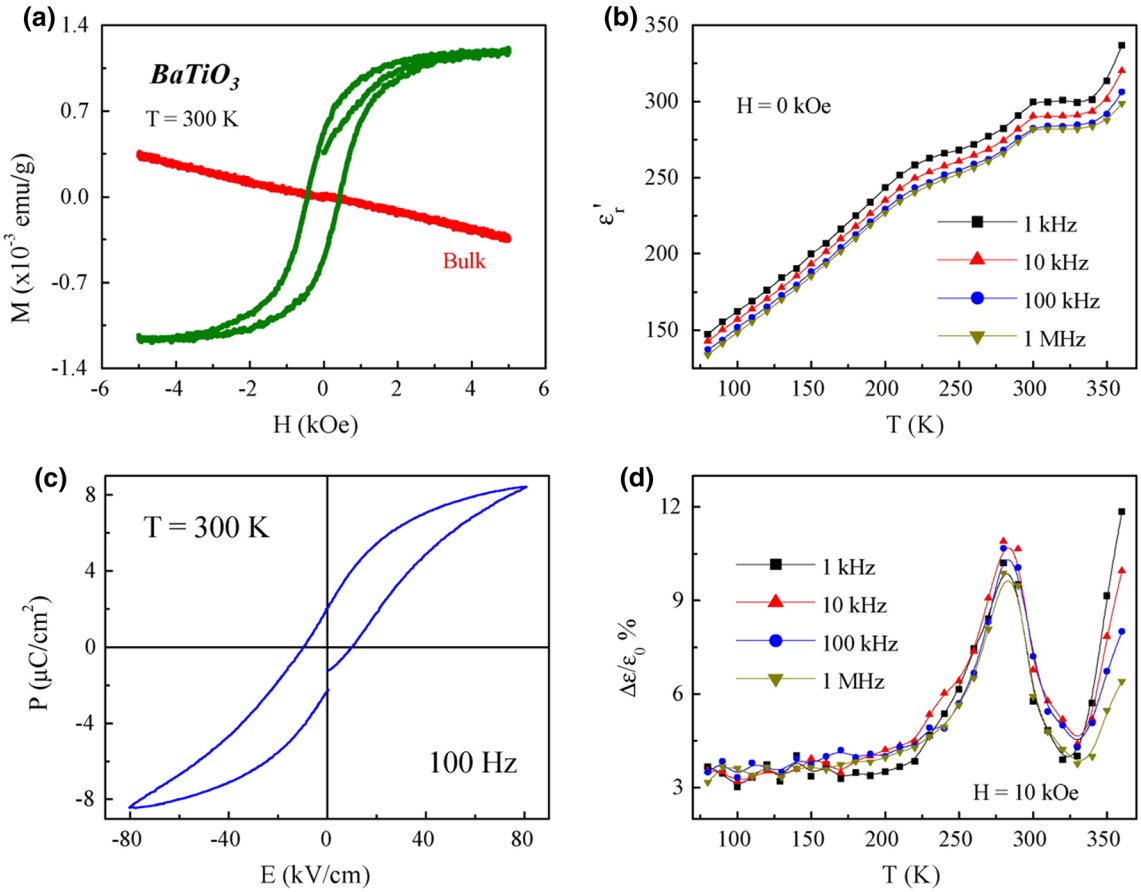

Fig. 4. (a) Magnetization curves of nanocrystalline and bulk $BaTiO_3$ showing ferromagnetic and diamagnetic behavior, respectively. (b) Dielectric constant of nanocrystalline $BaTiO_3$ showing anomalies indicating the ferroelectric phase transitions. (c) P-E hysteresis curve of nanocrystalline $BaTiO_3$. (d) Magnetocapacitance of nanocrystalline $BaTiO_3$ showing coupling of surface ferromagnetism with ferroelectricity. The figure is reprinted with permission from reference[45] under terms and conditions provided by Elsevier and Copyright Clearance Center. http://www.copyright.com/publishers/rightslink-permissions.

phases or clusters such as Cu, CuO, and Cu_2O are all antiferromagnetic (AFM). In 2005, Buchholz et al. experimentally reported the first room temperature ferromagnetism of nonmagnetic dopant Cu-doped ZnO thin films prepared by pulsed-laser ablation.[36] Their results obviously showed that Cu-doped ZnO thin films grown under conditions that produced *p*-type material exhibit room temperature ferromagnetism with a Curie temperature above 350 K while those grown under conditions that produced *n*-type ZnO show diamagnetic behaviour. As mentioned by the authors, the magnetic moment per copper atom was decreased as the copper concentration increased. In the same year, Duhalde et al. also reported the remarkable observation of significant room temperature ferromagnetism in Cu-doped TiO_2 thin films grown by pulsed laser deposition.[81] Interestingly, the magnetic moment estimated from the hysteresis loop of Cu-doped TiO_2 thin film was 1.5 μB per Cu atom. Later in 2006, Herng et al. studied the origin of room temperature ferromagnetism in copper-doped ZnO films grown on silicon substrates at room temperature by a filtered cathodic vacuum arc (FCVA).[82] They found that 5 at.% Cu-doped ZnO film exhibits room temperature ferromagnetism with saturation magnetization of 0.037μB/Cu atom. In their discussion, the origin of the ferromagnetism is principally attributed to the substitution of Cu^{2+} into Zn^{2+} sites. They stated that the presence of Cu ions in ZnO lattice induce the *p-d* hybridization between 3*d* of Cu and ZnO valence bands (O-*p* bands), which leads to a magnetic moment. Furthermore, the well separation of Cu–Cu ions in the *c* axis of ZnO structure could also contribute to the observed ferromagnetism.[82] Hou et al. reported significant room temperature ferromagnetism in nonmagnetic Cu-doped TiO_2 thin films grown by reactive magnetron sputtering.[83] The authors found that Cu-doped TiO_2 films annealed in air atmosphere did not show any magnetic properties, while those annealed in vacuum exhibit room temperature ferromagnetic properties with a Curie temperature near 350 K. The magnetic moment per copper atom was decreased as the copper concentration increased. The origin of the ferromagnetic behavior in these films was assigned to both oxygen vacancies and the distance between nearest-neighbor copper atoms. In the same context, room temperature ferromagnetism of Cu-doped ZnO ($Zn_{1-x}Cu_xO$, x = 0.05 and

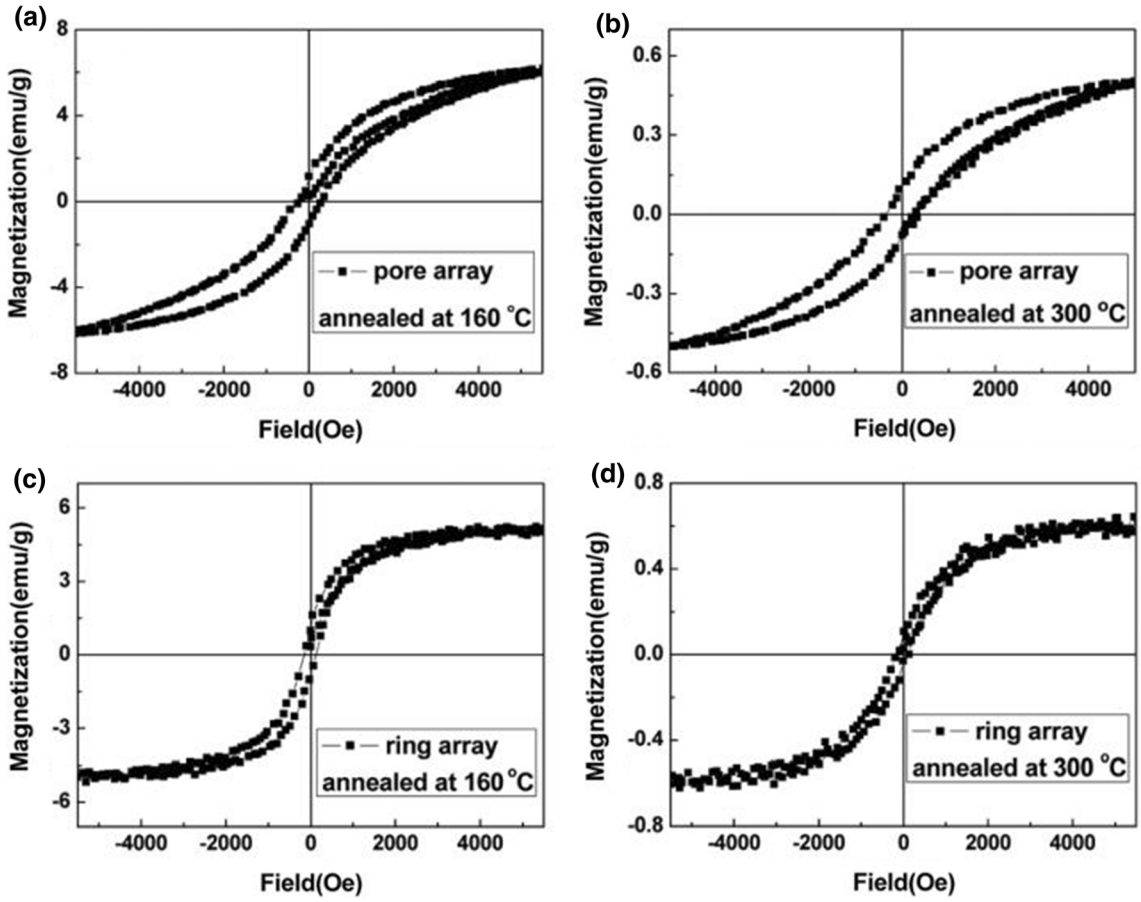

Fig. 5. Strong room temperature ferromagnetism of undoped ZnO nanostructure arrays prepared by colloidal template. The figure is reprinted with permission from reference[46] under terms and conditions provided by the Royal Society of Chemistry and Copyright Clearance Center. https://marketplace.copyright.com/rs-ui-web/mp.

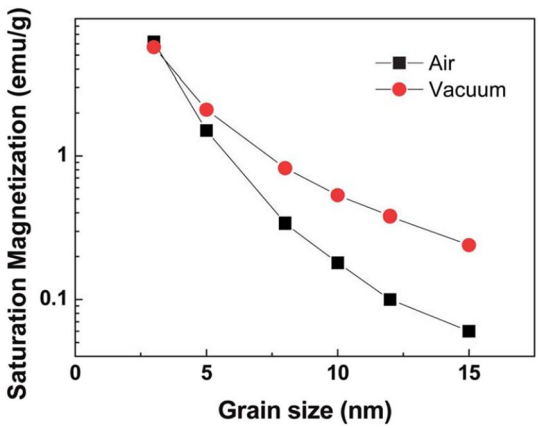

Fig. 6. Dependence of saturation magnetization on grain size of ZnO. The figure is reprinted with permission from reference[46] under terms and conditions provided by the Royal Society of Chemistry and Copyright Clearance Center. https://marketplace.copyright.com/rs-ui-web/mp.

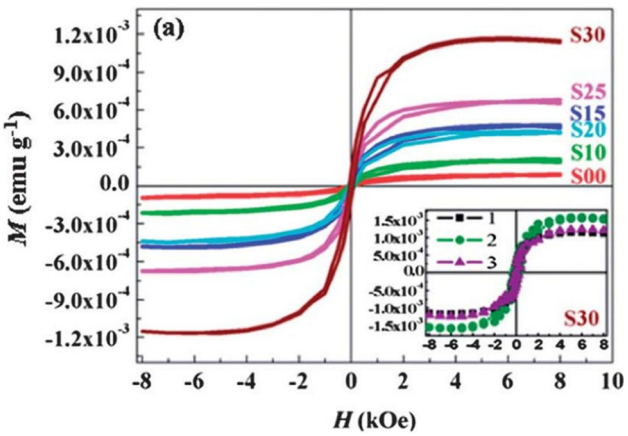

Fig. 7. Room temperature ferromagnetism of NaCl, S00, S10, S15, S20, S25 and S30 are NaCl powders planetary milled for different times 0, 1.0, 1.5, 2.0, 2.5, and 3.0 h, respectively. The inset shows the M–H curves of S30 every month. The figure is reprinted with permission from reference[50] under terms and conditions provided by the Royal Society of Chemistry and Copyright Clearance Center. https://marketplace.copyright.com/rs-ui-web/mp.

0.07) nanowire arrays embedded in an anodic aluminum oxide template was reported by Gao et al.[84] The magnetic hysteresis loop measurements indicated that both $Zn_{0.95}Cu_{0.05}O$ and $Zn_{0.93}Cu_{0.07}O$ nanowires reveal room temperature ferromagnetism and the $Zn_{0.93}Cu_{0.07}O$ nanowires annealed

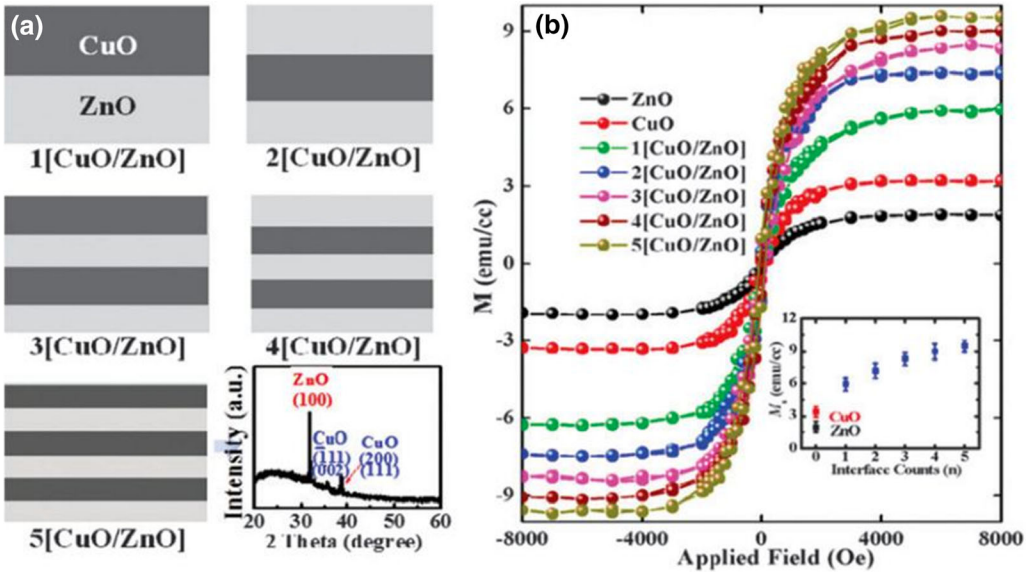

Fig. 8. (a) Schematic diagram for the CuO–ZnO film-heterostructures and the XRD result for the representative sample of 5[CuO–ZnO]. (b) M–H curves for the CuO–ZnO film heterostructures. The figure is reprinted with permission from reference[51] under terms and conditions provided by the Royal Society of Chemistry and Copyright Clearance Center. https://marketplace.copyright.com/rs-ui-web/mp.

Table I. Room temperature ferromagnetism in pure metal oxide semiconductors

Materials	Preparation method	Saturation magnetization	Year	Refs.
ZnO film	Pulsed laser deposition	3.5 emu/cm^3	2011	54
ZnO nanoflowers	Hydrothermal	0.069 emu/g	2010	55
ZnO single crystal	Hydrothermal	$\sim$ 0.007 emu/g	2019	56
ZnO film	Magnetron sputtering	110 emu/cm^3	2015	57
ZnO nanofibers	Electrospinning	0.039 emu/g	2014	58
ZnO film	RF sputtering	0.018 emu/cm^3	2013	59
ZnO rods	Co-precipitation	0.002 emu/g	2009	60
ZnO nanostructures	Solution plasma		2017	61
ZnO nanoparticles	Mechanical alloying	0.013 μB/f.u.	2014	62
ZnO film	Novel method of liquid ceramics	$0.8{\cdot}10^{-3}$ μB/f.u.	2011	63
ZnO nanoparticles	Pulsed laser deposition	10^{-6} emu	2012	64
ZnO single crystal	From MaTeck	2.5 $\times$ 10^{10} n/cm^2	2020	65
SnO_2 film	Sputtering	3.5 emu/cm^3	2019	66
SnO_2 film	Pulsed laser deposition	0.74 emu/cm^3	2017	67
SnO_2 nanocrystal	Sol-gel	10.856 $\times$ 10^{-2} emu/g	2017	68
SnO_2 nanoparticles	Sol-gel	6.64 $\times$ 10^{-2} emu/g	2019	69
TiO_2 film	Sol-gel	126 emu/cm^3	2014	70
TiO_2 thin films	Sputter deposition	40 emu/cm^3	2008	71
TiO_2 nanoparticles	Milling	10.33 $\times$ 10^{-3} emu/g	2015	72
ZnO thin film	RF sputtering	–	2019	73
ZnO thin film	Co-sputtering	1.62 emu/cc	2014	74
ZnO nanoparticles	Co-precipitation	0.018 emu/g	2009	75
ZnO nanorods	Vacuum annealing	0.35 emu/g	2017	76
CeO_2 nanoparticles	Thermal decomposition	0.062 emu/g	2015	77
Flowerlike CuO	Co-precipitation	0.022 emu/g	2010	78
CuO nanograins	Electrical resistive heating	3 $\times 10^{-2}$ μB/f.u	2013	78
CeO_2 nanoparticles	Precipitation	0.018 emu/g	2010	79
CuO thin film	Magnetron sputtering	12 emu/cc	2016	80

in vacuum exhibit an improvement in ferromagnetism.

Recently, Alla et al. studied ferromagnetic behaviour of Cu-doped CeO_2 ($Cu_xCe_{1-x}O_2$, x = 0.01, 0.03 and 0.05) nanostructures prepared by microwave

refluxing.[85] The results showed that all doped CeO_2 samples have room temperature ferromagnetic behaviors with saturation magnetization of 0.0027, 0.012 and 0.001 Am^2/kg for x = 0.01, 0.03 and 0.05, respectively. Similarly, room temperature ferromagnetism in Cu-doped ZnO nanofibers prepared by electrospinning was studied by Chen et al.[86] As mentioned by the authors, 8% Cu-doped ZnO sample (by thermal diffusion) exhibits a high saturation magnetization value equal to 1.35 emu/g as shown in Fig. 9. The ferromagnetic behavior induced by copper as a nonmagnetic dopant encouraged scientists to examine other nonmagnetic elements to induce room temperature ferromagnetism in different oxides.

The observation of room temperature ferromagnetism in Sc-doped ZnO by Venkatesan et al. is quite surprising,[87] since neither Zn^{2+} ($3d^{10}$) nor Sc^{3+} ($3d^0$) are magnetic ions, and the 3d level of zinc lies well below that of scandium, so no electron transfer to scandium is seen. The magnetic moment detected in 5 at.% Sc-doped ZnO is 0.3 μB/Sc.[87] The effect of Ti doping on the room temperature ferromagnetism of nano-crystalline SnO_2 ($Sn_{1-x}Ti_xO_2$, x = 0.00, 0.02, 0.05 and 0.07) prepared by sol–gel method without any surfactant or dispersant material was investigated.[88] The magnetic results confirmed that the pure and 2% Ti-doped SnO_2 exhibit perfect room temperature ferromagnetism (RTFM) while 5% and 7% Ti-doped samples show a weak ferromagnetism with diamagnetic contribution. On the other hand, Bhowmik et al. studied the magnetic properties of α-Fe_2O_3 and Ti doped α-Fe_2O_3 thin films grown on different substrates at 400 °C by using pulsed laser deposition.[89] After that, these films were heated in the temperature range of 600–730 °C either in air or vacuum. They found that some films possess room temperature ferromagnetism or canted antiferromagnetism which may be useful for spintronics applications.

Room temperature ferromagnetism in Y-doped HfO_2 ($Hf_{1-x}Y_xO_{2-\delta}$, $0.05 \leq x \geq 0.2$) nanoparticles obtained by metathesis synthesis was investigated by Dohcević-Mitrović et al.[90] Structural analysis of these samples shows that there are phase transformations from monoclinic to tetragonal and cubic phases by increasing the Y content in HfO_2 nanopowders. The ferromagnetic hysteresis loops of Y-doped HfO_2 samples are dependent on crystal structure changes. The saturation magnetization value (Ms) of pure HfO_2 was found to be 2.2×10^{-3} emu g^{-1}. The value of the saturation magnetization was increased by addition of 5 at% Y-doped HfO_2 and reaches its maximum of 2.9×10^{-3} emu g^{-1} for 10 at% doped HfO_2 sample. Another study on Y-doped CeO_2 (0-15%) nanoparticles synthesized by precipitation method showed room temperature ferromagnetism in these compositions and the authors related it to the presence of defects.[91] In case of nonmagnetic Zr element, Ma et al. investigated the ferromagnetic properties of Zr-doped CeO_2 synthesized by a hydrothermal method.[92] The authors clearly showed that $Ce_{0.94}Zr_{0.06}O_2$ sample exhibits a ferromagnetic hysteresis loop with saturation magnetization and remanent magnetization of 0.97×10^{-3} emu/g and 0.09×10^{-3} emu/g, respectively. This ferromagnetic behaviour was explained based on structure distortion and oxygen defects induced by Zr doping on substitutional sites. Another work on Zr-doped ZnO ($Zn_{1-x}Zr_xO$, x = 0.00-0.10) prepared by formal solid-state reaction showed that $Zn_{0.96}Zr_{0.4}O$ composition possesses a perfect ferromagnetic behavior with maximum saturation magnetization of 9.6×10^{-4} emu/g.[93] Specifically, the Zn^{2+} ion as a dopant has full 3d orbital ($3d^{10}$) with no unpaired electrons. However, Liu et al. synthesized $Sn_{1-x}Zn_xO_2$ nanorods with varying Zn concentration (x = 0, 0.04, 0.08, 0.12, 0.16, 0.20) by a solvothermal method and investigated their magnetic properties.[94] The X-ray diffraction analysis shows that Zn ions have been

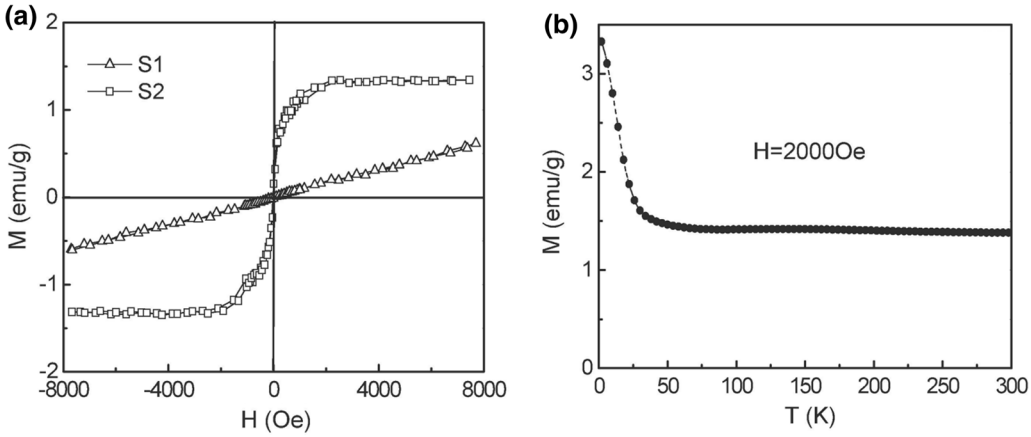

Fig. 9. M-H curves of the Cu-doped ZnO nanofibers recorded at room temperature (a), M-T curve of the Cu-doped ZnO nanofibers (b). The figure is reprinted with permission from reference[86] under terms and conditions provided by Elsevier and Copyright Clearance Center. http://www.copyright.com/publishers/rightslink-permissions.

successfully substituted the Sn sites in the SnO_2 lattice without forming secondary phases. Interestingly, all Zn-doped samples reveal ferromagnetic performance at room temperature. The measured values of saturation magnetization (Ms) and coercivity of 4 at% doped SnO_2 are 0.44×10^{-3} emu/g and 180 Oe, respectively. By increasing Zn concentration to 8 at%, the saturation magnetization is markedly improved (0.85×10^{-3} emu/g). They attributed the observed room temperature ferromagnetism in Zn-doped SnO_2 samples to the doping-induced V_{Sn} defects. On the other hand, room temperature ferromagnetism of Zn-doped SnO_2 flower-like microparticles synthesized by the hydrothermal method was evaluated by Paraguay-Delgado et al.[95] The morphological analysis of these nanoparticles displays progressive changes from truncated rods to sharp needles due to Zn doping. The magnetic measurements reveal that pure SnO_2 has weak ferromagnetism while Zn-doped samples exhibit enhanced ferromagnetic ordering. The authors found that pure and 2 and 5 at.% Zn-doped SnO_2 possess saturation magnetization values of 0.027, 0.31 and 0.42 kAm^{-1}, respectively.

Some research groups studied the impact of Cd on the magnetic behavior of some metal oxides ZnO.[96–98] In these studies, Debbichi et al. detected room temperature ferromagnetism in pure and Cd-doped ZnO thin films grown on a c-plane sapphire substrate by metal organic chemical vapor deposition.[96] As reported by the authors, pure, 0.7%, 3%, and 4.6% Cd-doped ZnO thin films exhibit saturated moments of 0.10, 0.22, 0.31 and 0.42 emu/ cm^3, respectively. Their theoretical study based on density functional theory revealed that Cd replacement at Zn sites contributes to the long-ranged ferromagnetism in ZnO due to lowering the formation energy of Zn vacancies which stabilize Zn vacancies from which the magnetic moments originate. Another group synthesized Cd-doped ZnO thin films on a c-plane sapphire substrate by metal–organic chemical vapor deposition (MOCVD) at 380 °C.[97] The M-H hysteresis loop of the prepared Cd-doped ZnO thin film at room temperature displays a perfect ferromagnetic behavior with remanence (Mr) value equal to 0.0262 emu/ cm^3, and coercive field (Hc) of 52 Oe. Ramya et al. used chemical precipitation in synthesizing undoped and Cd-doped CuO nanoflakes and then investigated their magnetic properties.[98] All these samples exhibited ferromagnetic properties and the ferromagnetism in CuO nanocrystals is significantly improved by substitution of Cu sites by Cd ions. With respect to Ag dopant, room temperature ferromagnetism was reported for Ag-doped ZnO films prepared by DC magnetron sputtering by Xu et al.[99] In the same way, the impact of nonmagnetic Ag doping on the magnetism of ZnO was investigated by Ali et al.[100] Experimentally, they noticed room temperature ferromagnetism in Ag-doped ZnO samples with Ag content varied from 0.03% to 10%. In these systems, the authors stated that zinc vacancy (V_{Zn}) improves the ferromagnetic ordering while oxygen vacancy (V_O) hinders the ferromagnetism.

Nonmagnetic Post-Transition Elements

Al, In and Bi are nonmagnetic dopants belonging to post-transition elements. Room temperature ferromagnetism in epitaxial Al-doped SnO_2 films fabricated by radio-frequency magnetron sputtering was studied by Yang et al.[101] The saturation magnetization of these films was enhanced by Al_{Sn} doping and the maximum value was observed in the $Sn_{0.98}Al_{0.02}O_2$ film. The localized holes introduced by incorporation of Al ions into Sn sites contributes to the magnetic moment. Lu et al. investigated the influence of Al-doping on the structural, optical, and magnetic properties of ZnO nanoparticles synthesized by a hydrothermal method and then annealed in air at different temperature.[102] The X-ray diffraction analysis of all samples showed the formation of hexagonal ZnO wurtzite structure without any impurities. The authors found that all samples exhibit room temperature ferromagnetism and annealing in air enhances the saturation magnetization value particularly at 160 °C. The Al-doped ZnO sample annealed at 160 °C exhibits a saturation magnetization value equal to 3.97×10^3. Indium (In) is one the nonmagnetic element which was utilized to induce room temperature ferromagnetism in ZnO and SnO_2.[103,104] Liu et al. studied the optical and magnetic properties of pure and indium-doped ZnO ($Zn_{0.97}In_{0.03}O$ and $Zn_{0.94}In_{0.06}O$) nanowires prepared by vapor phase transport process.[103] The magnetic measurements of these systems revealed that pure ZnO nanowires are diamagnetic while $Zn_{0.97}In_{0.03}O$ and $Zn_{0.94}In_{0.06}O$ nanowires exhibit intrinsic ferromagnetism at room temperature. They found that the coercive field and the magnetic moment increase with increasing indium content in ZnO nanowires. The authors attributed the ferromagnetic ordering in these samples to oxygen vacancies induced by indium doping and support their conclusion by photoluminescence (PL) measurements. Similarly, the ferromagnetic behavior of pure and indium-doped SnO_2 (2, 5 and 25%) nanocrystalline thin films fabricated using sol-gel technique was studied by Singh et al.[104] Both pure and 5% In-doped SnO_2 thin films reveal room temperature ferromagnetism but indium doping enhances the saturation magnetization value compared to that of the pure sample. In these samples, the ferromagnetic behavior was assigned to the defects and oxygen vacancy formation.

Also, Bi, a heavy metal dopant, was used to improve the magnetic properties of zinc oxide nanowires. Kazmi et al. used a hydrothermal method to fabricate the pristine and Bi-doped ZnO nanowires (NWs) grown on glass and Si substrates.[105] The magnetic properties of undoped and doped ZnO samples showed room temperature

ferromagnetic behavior. The authors found that the saturation magnetization of Bi-doped ZnO was higher compared to that of the pristine ZnO samples until 1% Bi content. In the same context, another study on magnetic properties of Bi-doped ZnO ($ZnBi_{0.03}O_{0.97}$) thin film grown using pulsed laser deposition was carried out by Lee et al.[106] This thin film showed a room temperature ferromagnetic hysteresis loop with remnant magnetization = 7.218×10^{-5} emu/g and saturation magnetization value of 7.223×10^{-4} emu/g. There are many studies on nonmagnetic transition and post-transition elements that we attempt to summarize in detail in Table II.

Nonmagnetic Alkali Elements

The elements of alkali earth metals (Li, Na and K) represent another group of nonmagnetic dopants which were used to induce or enhance the room temperature ferromagnetism of metal oxides. In 2009, S. Chawla et al. observed room temperature ferromagnetic properties in Li-doped p-type luminescent ZnO nanorods prepared by solid-state reaction.[132] Among all samples, A typical room temperature ferromagnetic hysteresis loop was detected for a 2 at.% Li-doped ZnO sample with retentivity of 9.62 memu/g and coercivity of 166.97 Oe. The authors stated that the synthesis method is an important factor for the occurrence of *p*-type conduction and ferromagnetism in Li-doped ZnO. The observed ferromagnetic behavior was explained by the incorporation of Li ions into ZnO creating random potential and inducing a magnetic moment on oxygen atoms whose orbital is considered correlated. Later, in 2010, the magnetic properties of Li-doped ZnO thin films grown by pulsed laser deposition was investigated by Yi et al.[133] The authors demonstrated both theoretically and experimentally that cation vacancy may be the origin of ferromagnetism in Li-doped ZnO. They stated that the insertion of Li ions into the ZnO lattice creates holes and reduces the formation energy of Zn vacancy. In their study, 8 at.% Li-doped ZnO showed the maximum saturation magnetization value. Kung et al. studied the effect of Li doping at different concentrations on the magnetic properties of ZnO nanorods prepared by a hydrothermal method.[134] The structural analyses of these compositions confirmed the formation of pure single-phase ZnO with wurtzite hexagonal structure. All samples exhibited room temperature ferromagnetism with enhanced saturation magnetization values due to Li

Table II. Room temperature ferromagnetism induced by nonmagnetic transition and post-transition dopants in metal oxide semiconductors

Materials	Dopant	Preparation method	Saturation magnetization or magnetic moment (best sample)	Reference
ZnO	Cu	Hydrothermal route	2.75 emu/ cm^3	107
ZnO	Cu	Radio frequency magnetron sputtering	0.12 μ_B/Cu	108
ZnO	Cu	Chemical vapor deposition	0.22 emu/g	109
ZnO	Cu	Ultrasound assisted solid state	0.00272 emu/g	110
ZnO	Cu	Electrodeposition	1.82 μ_B/Cu	111
ZnO	Cu	Spin coating	1.1 emu/g	112
ZnO	Cu	Hydrothermal	0.012 emu/g	113
ZnO	Cu	Co-precipitation	0.0065 emu/g	114
SnO_2	Cu	Sol-gel	0.20 emu/g	115
SnO_2	Cu	Thermal evaporation	15.65 emu/g	116
TiO_2	Cu	Sol-gel	0.166 emu/g	117
TiO_2	Cu	Two-step anodization	0.013 emu/g	118
CeO_2	Cu	Solvothermal	1.58 μ_B/Cu	119
In_2O_3	Cu	Ion source/frequency sputtering	5.8×10^{-5} emu/g	120
NiO	Cu	Electrodeposition	0.000292 emu/g	121
SnO_2	Zn	Microwave irradiated solvothermal	10.2408×10^{-3} emu/g	122
ZnO	Ag	Electrochemical deposition	0.023 emu/g	123
SnO_2	Al	Sol-gel	7.3×10^{-3} emu/g	124
ZnO	Al	Hydrothermal	10.66×10^{-4} emu/g	125
SnO_2	Al	Gel combustion	0.33×10^{-3} emu/g	126
TiO_2	Sn	Hydrothermal	129.56×10^{-3} emu/g	127
ZnO	Sn	Hydrothermal	0.045 emu/g	128
ZnS	Sn	Electron beam evaporation	18×10^{-6} emu/g	129
ZnO	Bi	Co-precipitation	0.5594 emu/g	130
ZnO	Bi	Chemical vapor deposition	1.08 emu/g	131

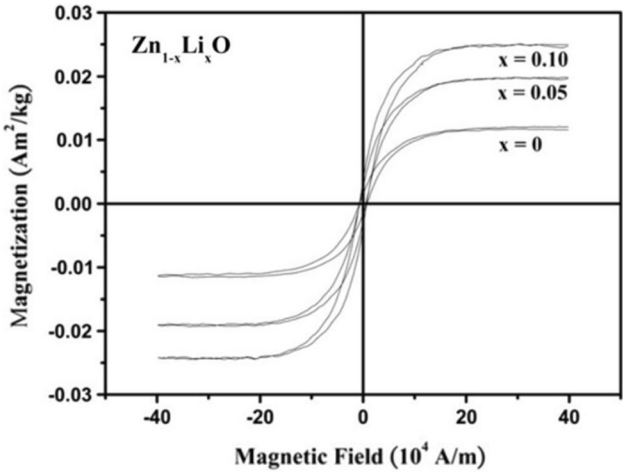

Fig. 10. Room temperature magnetization loops of the $Zn_{1-x}Li_xO$ nanorods. The figure is reprinted with permission from reference[134] under terms and conditions provided by Elsevier and Copyright Clearance Center. http://www.copyright.com/publishers/rightslink-permissions.

doping. As shown in Fig. 10, the saturation magnetization was estimated to be 0.012, 0.019 and 0.025 Am^2/kg for ZnO, $Zn_{0.95}Li_{0.05}O$ and $Zn_{0.9}Li_{0.1}O$ nanorods samples, respectively.

In the case of In_2O_3, Cao et al. used the sol–gel method in synthesizing Li-doped In_2O_3 ($(In_{1-x}Li_x)_2O_3$, x = 0, 0.005, 0.01, 0.02, 0.05, 0.07) nanoparticles and then investigated their magnetic properties.[135] The prepared samples of Li-doped In_2O_3 revealed ferromagnetic properties at room temperature with maximum saturation magnetization 1.25 $\times 10^{-3}$ emu/g at 2 at.% Li content. The authors attributed the ferromagnetic coupling in these samples to Li_{In}-O_{NN}-V_{In}-O_{NN}-Li_{In} chains. Recently, the large room temperature ferromagnetism of Li-doped ZnO (1, 5 and 10%) nanoparticles synthesized by chemical precipitation was reported.[136] The magnetic measurements showed that the 1% Li-doped ZnO sample has a perfect ferromagnetic hysteresis loop with maximum coercivity and saturation magnetization of 1570 Oe and 0.055 emu/gm. This ferromagnetic behavior was assigned to Zn vacancies, Li interstitial and Li substitution vacancies but not from oxygen vacancies.

With respect to the Na dopant, the room temperature ferromagnetism of Na-doped SnO_2 nanoparticles based on experimental and first-principles studies was presented by Wang et al.[137] Initially, they found that the saturation magnetization increases with increasing Na content until 4% and then decreases. The $Sn_{0.96}Na_{0.04}O_2$ structure exhibits the largest saturation magnetization of 1.1 memu/g. In the same context, the magnetic properties of K-doped SnO_2 synthesized by the sol–gel method was investigated by Zhou et al.[138] A single phase with a rutile structure without any impurities was detected in these samples. A perfect ferromagnetic hysteresis loop was seen for the 8% K-doped

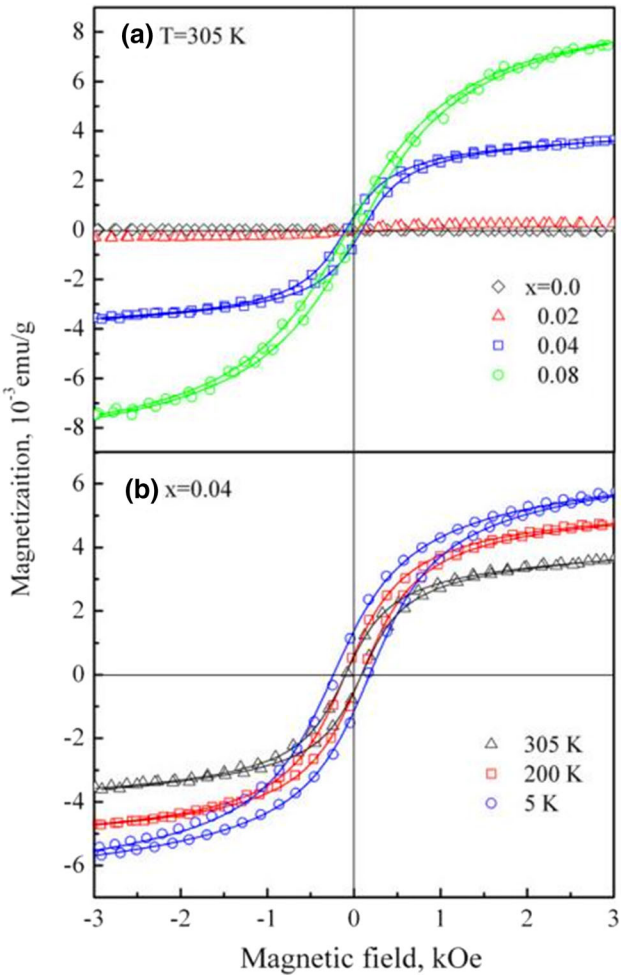

Fig. 11. Room temperature magnetization curves of $Sn_{1-x}K_xO_2$ nanocrystals, and (b) the magnetization curves of $Sn_{0.96}K_{0.04}O_2$ nanocrystals at temperature of 5 K, 200 K, and 305 K. The figure is reprinted with permission from reference[138] under terms and conditions provided by Elsevier and Copyright Clearance Center. http://www.copyright.com/publishers/rightslink-permissions.

SnO_2 sample with highest saturation magnetization equal to 9.2 $\times$ 10^{-3} emu/g, as seen in Fig.11. Huang et al. reported room temperature ferromagnetism in epitaxial p-type K-doped ZnO films prepared by RF-magnetron sputtering.[139] Remarkably, as mentioned by the authors, the 8% K-doped film possesses the maximum saturation magnetization of 8 emu/ cm^3, and the thermal annealing of film samples in air atmosphere can stabilize the ferromagnetic behavior, as seen in Fig. 12. Based on first-principles calculations the ferromagnetic nature in K-doped ZnO films is ascribed to the strong p–p interaction between the unpaired 2p electrons at O sites.

Nonmagnetic Alkaline Earth Elements

The nonmagnetic alkaline earth group elements which include Be, Mg, Ca, Sr, Ba, and Ra. Panigrahi et al. studied the influence of Mg ions on magnetic properties of NiO nanoparticles prepared by

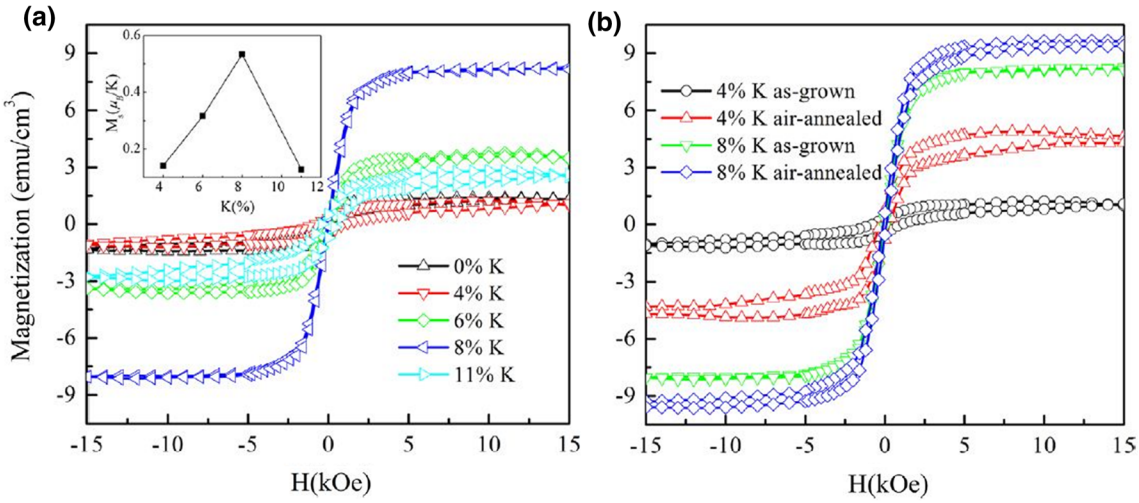

Fig. 12. (a) Room temperature M–H loops of the K-doped ZnO films, and the inset is the magnetic moment per K as a function of the K concentration and (b) the M–H loops of the as-grown and air-annealed (700 °C, 1 h) for the 4% and 8% K-doped films at 300 K. The figure is reprinted with permission from reference[139] under terms and conditions provided by Elsevier and Copyright Clearance Center. http://www.copyright.com/publishers/rightslink-permissions.

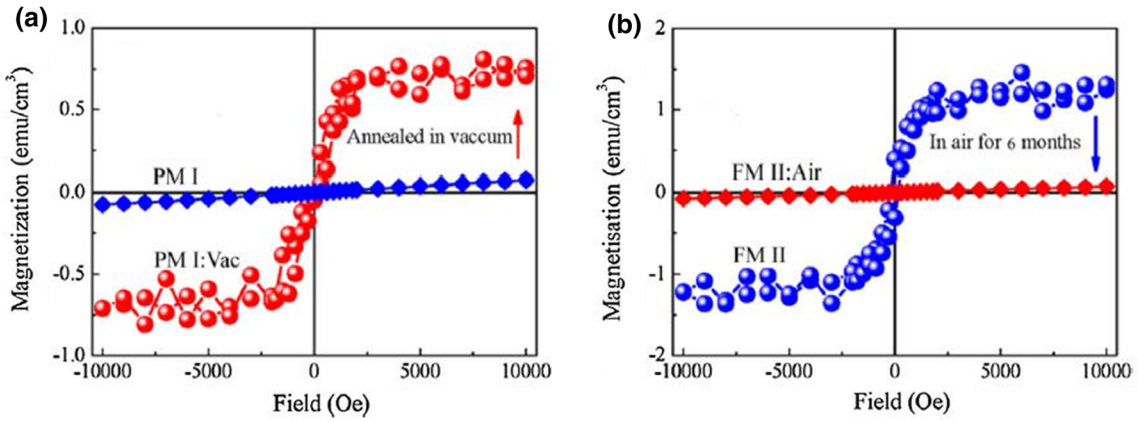

Fig. 13. Room temperature magnetization vs. applied magnetic field curves. (a) PM I (paramagnetic) and PM I:Vac (as-deposited and annealed); (b) FM II (ferromagnetic) and FM II:Air (as-deposited and aged). The figure is reprinted with permission from reference[142] under terms and conditions provided by Elsevier and Copyright Clearance Center. http://www.copyright.com/publishers/rightslink-permissions.

chemical method.[140] The magnetic behavior of the prepared samples displayed weak room temperature ferromagnetism along with the dominance of background antiferromagnetism. In another work, the ferromagnetism in epitaxial Mg-doped SnO_2 thin films prepared by radio-frequency magnetron sputtering was examined at room temperature.[141] 6% Mg-doped SnO_2 thin film exhibits room temperature ferromagnetism with a saturation magnetization = 6.9 emu/ cm^3. They attributed the ferromagnetic nature to hole formation due to Mg doping. Interestingly, robust room temperature ferromagnetism was reported for nonmagnetic Mg-doped ZnO films grown by pulsed laser deposition as illustrated in Fig. 13.[142] Their results show that Mg doping induces room temperature ferromagnetism in ZnO with a maximum saturation magnetization of 2.5 emu/cm^3. Dimri et al. investigated the ferromagnetic properties of Ca- and Mg-doped zirconia bulk and thin film samples prepared by pulsed laser deposition.[143] Both $Zr_{0.86}Mg_{0.14}O_2$ and $Zr_{0.84}Ca_{0.16}O_2$ samples display ferromagnetic performance with saturation magnetization of 0.012 and 0.0335 emu/g, respectively.

Nonmagnetic strontium (Sr) was utilized to tune the magnetic properties of TiO_2 and SnO_2. Rajamanickam et al. used hydrolysis to synthesize undoped and Sr-doped TiO_2 nanoparticles with evolution of their magnetic properties.[144] They observed that Sr doping greatly enhances the room temperature ferromagnetism of TiO_2, Fig. 14. The saturation magnetization and coercivity of best composition ($Ti_{0.95}Sr_{0.05}O_2$) were 7.47×10^{-3} emu/g, 280.68 G, respectively. On the other hand, Wang et al. observed oxygen vacancy-mediated room temperature ferromagnetic properties in Sr-doped

SnO_2 ($Sn_{1-x}Sr_xO_2$, x = 0.00, 0.02, 0.03, 0.05, 0.06, 0.08) nanoparticles synthesized via the sol–gel technique.[145] Both pure and Sr-doped SnO_2 nanoparticles show room temperature ferromagnetism with largest the saturation magnetization of 6.98 × 10^{-4} emu/g reported for $Sn_{0.95}Sr_{0.05}O_2$ sample. The authors noticed a strong relation between oxygen vacancy defects and ferromagnetism. Other studies related to room temperature ferromagnetism by alkali and alkaline elements are tabulated in Table III.

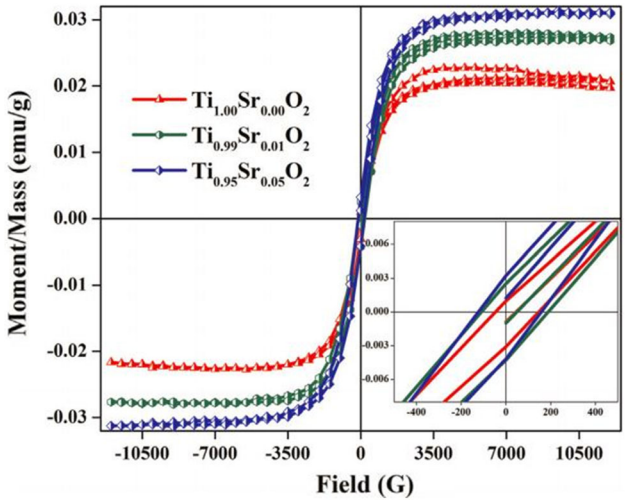

Fig. 14. VSM spectra of $Ti_{1-x}Sr_xO_2$ (x = 0.00, 0.01, and 0.05) nanoparticles. The figure is reprinted with permission from reference[144] under terms and conditions provided by Elsevier and Copyright Clearance Center. http://www.copyright.com/publishers/rightslink-permissions.

Nonmagnetic Nonmetal Elements

Nonmetal elements such as B, C and N mostly lack the characteristics of a metal. In 2008, Yang et al. performed first-principles calculations on C-doped TiO_2 structures to show the possibility of achieving room temperature ferromagnetism.[162] Their work demonstrates that each C has spin-polarized 2p states in the band gap generating a magnetic moment of 2.0μ_B. Later in 2009, Ye et al. experimentally studied the ferromagnetic properties at room temperature of carbon-doped TiO_2 synthesized by solid-state reaction and sintered in argon or nitrogen atmosphere.[163] They noticed that all the samples exhibited room temperature ferromagnetic but with high saturation magnetization for samples sintered under argon atmosphere. C-doped TiO_2 with nominal carbon concentration of 5 mol% sintered in argon atmosphere exhibits magnetic moment per carbon in carbide state equal to 0.0236 μB with saturation magnetization of 8.4 × 10^{-4} emu/g. In the same context, the as prepared C-doped TiO_2 nanoparticles by a hydrothermal method showed a ferromagnetic performance with maximum saturation of 0.038 emu/g.[164] Ye et al. have used the solid-state reaction to synthesize n-type carbon-doped ZnO with intrinsic room temperature ferromagnetism.[165] They found that the 15% C-doped ZnO sample has the highest saturation magnetization value of 15.2 × 10^{-4} emu/g. The magnetic properties of 1, 2 and 3 at.% C-doped ZnO thin films prepared by electron beam evaporation were studied by Akbar et al.[166] X-ray diffraction analysis confirmed the formation of ZnO wurtzite structure without any impurities. As depicted in Fig. 15, all these films clearly revealed ferromagnetism at room temperature with the strongest

Table III. Room temperature ferromagnetism induced by nonmagnetic alkali and alkaline dopants

Materials	Dopant	Preparation method	Saturation magnetization or magnetic moment (best sample)	References
SnO_2	Li	Radio frequency magnetron sputtering	7.9 emu/ cm^3	146
SnO_2	Li	Solvothermal	0.0054 ± 0.0003 emu g^{-1}	147
ZnO	Li	Sol-gel	~0.03 emu/g	148
ZnO	Li	Sol-gel	0.02936 emu/g	149
ZnO	Li	Sol–gel dip coating	8.2 × 10^{-5} μB	150
ZnO	Li	Chemical co-precipitation	~2.5 emu/g	151
ZnO	Li	Hydrothermal	0.0405 emu/g	152
ZnO	Li	Hydrothermal	0.060 emu/g	153
ZnO	K	Combustion	~ 0.006 emu/g	154
ZnO	K	Two-step anodization	0.38 emu/g	155
ZnO	Na	Sol-gel	27 $mA{\cdot}m^2{\cdot}kg^{-1}$	156
ZnO	Na	Hydrothermal	~ 0.008 emu/ cm^3	157
ZnO	Na	Pulse laser deposition	~ 2.02 emu/ cm^3	158
ZnO	Na	Hydrothermal	2 emu/ cm^3	159
ZnO	Mg	Chemical	1.05 × 10^{-3} emu/g	160
TiO_2	Mg	Sol-gel	2.73 ×10^{-3} emu/g	161

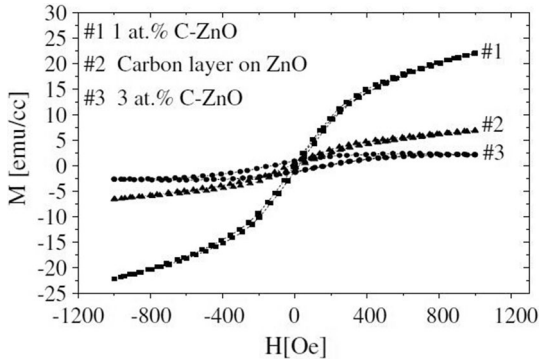

Fig. 15. Room temperature hysteresis loops for (#1) 1 at.% C-doped ZnO, (#2) 3 at.% C-doped ZnO films and (#3) C-coating on ZnO thin film. The figure is reprinted with permission from reference[166] under terms and conditions provided by Elsevier and Copyright Clearance Center. http://www.copyright.com/publishers/rightslink-permissions.

magnetic moment (~ 22.5 emu/cc) in the case of 1 at.% C doping.

Nanoneedle-shaped carbon-doped ZnO was fabricated by ion beam irradiation.[167] Remarkably, this structure showed ferromagnetic behavior at room temperature with enhanced saturation magnetization 3.04 emu/cm^3 compared to the pure sample (1.24 emu/cm^3). On the other hand, hexagonal and round nanoparticles of carbon-doped ZnO prepared by sol-gel technique exhibited a ferromagnetic performance as reported by Dung et al.[168] Carbon-doped ZnO powders with nominal concentrations of 0, 1, 3, 5, 8 and 10 mol% were synthesized by mechanical milling assisted by solid-state reaction.[169] As mentioned by the authors, 3 mol% carbon doped ZnO displayed the maximum saturation magnetization. Ruan et al. investigated the magnetic properties of carbon-doped In_2O_3 thin films prepared on Si (100) substrates by RF-magnetron co-sputtering.[170] Enhanced room temperature ferromagnetism is seen in these samples with 4.8 emu/g as a maximum saturation magnetization. The authors assigned the magnetic properties of these films to defects in In_2O_3:C systems. In the same way, Khan et al. studied the influence of annealing on the ferromagnetic properties of In_2O_3:C thin films synthesized by co-sputtering.[171] Interestingly, C-doped In_2O_3 thin films exhibited room temperature ferromagnetism with maximum magnetization reached to 5.7 emu/cm^3 at 3.4 at% C content. Annealing of these films in oxygen environment resulted in a decrease in the magnetization, indicating the crucial role of oxygen vacancies in the films.

In the case of nitrogen (N), Shen et al. used RF-magnetron sputtering technique to prepare pure In_2O_3 and N-doped In_2O_3 films with a thickness of about 400 nm on (001) Si and ultra-white glass substrates.[172] Unusually, N-doped In_2O_3 films showed perfect room temperature ferromagnetism and the saturated magnetization of the films monotonically increases with increasing N doping concentration. Specifically, 5 at% N-doped In_2O_3 film exhibited the highest saturation magnetic moment of 0.6 emu/cm^3. On the other hand, room temperature ferromagnetic properties have been experimentally detected in N-doped rutile TiO_2 films prepared by pulse laser deposition under N_2O atmosphere with magnetic moment of approximately 0.9 μB per N atom.[173] Similarly, Gómez-Polo studied the room temperature ferromagnetism of pure and N-doped TiO_2 nanoparticles obtained by sol-gel technique.[174] As reported by the authors, pure TiO_2 has shown a paramagnetic-like behavior while the N-doped TiO_2 sample exhibits enhanced room temperature ferromagnetic after post-annealing treatments with saturation magnetization = 3.49 $\times 10^{-3}$. In other research, the nanowire structure of both undoped and N-doped TiO_2 samples prepared by a hydrothermal method revealed room temperature ferromagnetism.[175] The estimated values of the saturation magnetizations were 0.007 and 0.042 emu/g for pure and N-doped TiO_2, respectively. Their results indicated that the oxygen vacancies and crystallinity play essential role in the enhanced room temperature ferromagnetism of N-doped TiO_2 nanowires.

Gómez-Polo showed that the nanoparticles of nitrogen-doped TiO_2 synthesized by the sol–gel method display ferromagnetic features at room temperature.[176] Remarkably, N doping and post-annealing of samples in vacuum greatly enhance the ferromagnetic properties and increase the saturation magnetization from 0.001 to 0.008 emu/g. In the case of ZnO, Wang et al. investigated the room temperature ferromagnetism of N-doped ZnO thin films deposited using magnetron sputtering.[177] They found room temperature ferromagnetic hysteresis loops for all N-doped ZnO thin films. The influence of UV irradiation on the saturation magnetization of nitrogen-doped ZnO films was investigated by Yu et al.[178] The authors found that the saturated room temperature ferromagnetism in N-doped ZnO increases significantly after ultraviolet light irradiation for 5 min. N-doped SnO_2 films synthesized by oxidative annealing of sputtered SnN_x films with various temperatures exhibited enhanced ferromagnetism due to N doping with an interesting saturation magnetization value = 10.1 emu/cm^3.[179] Based on theoretical calculations of density-functional theory, this ferromagnetic behavior is assigned to double exchange mechanism through the p–p interaction.

Li et al. investigated the room temperature ferromagnetism of C-/N-/O-implanted MgO single crystals prepared by arc melting and packaged in a vacuum.[180] They found that all samples with high-dose implantation displayed room temperature ferromagnetic hysteresis loops. The ferromagnetic behavior at room temperature in O-implanted samples was ascribed to the presence of Mg vacancies while the introduction of C or N played a more active role in the room temperature ferromagnetism than Mg vacancies. Referring to boron (B) as a dopant, Yılmaz et al. studied the effect of defects on

room temperature ferromagnetism of B diffused into ZnO microrods grown on glass substrates by spray pyrolysis.[181] The magnetic measurements demonstrated that B-doped ZnO samples revealed room temperature ferromagnetism related to defects in ZnO structure. Experimentally and theoretically, Xu et al. reported room temperature ferromagnetism in single-phase boron-doped ZnO films prepared by pulsed laser deposition.[182] As found by the authors, increasing the boron component from 0% to 6.8% leads to monotonic increases in saturation magnetization from 0 to 1.5 emu/cm^3. The theoretically study of these films revealed that the ferromagnetism in the B-doped ZnO originates from the induced magnetic moment of oxygen atoms in the nearest neighbor sites to B–Zn vacancy pairs. Table IV summarizes other studies on ferromagnetic properties of nonmetal dopants used to dope metal oxides.

Brief Vision of Possible Mechanisms of d^0 Ferromagnetism

The room temperature ferromagnetism which originates in completely filled or unfilled d-orbitals or f-orbitals is generally called d^0 ferromagnetism and is a critical field of study for the scientific community and is considered to be one of the most interesting and challenging phenomena.[194,195] Great efforts have be done to understand the possible mechanisms which inducing the room temperature ferromagnetism in undoped or in doped with nonmagnetic dopants. During recent years, the mechanism of room temperature d^0 ferromagnetism which is noticed in many oxides, sulfides, and other semiconductors, principally in nanoscale size is linked with intrinsic defects or impurities without participation of the conventional 3d or 4f magnetic ions.[166,196] Coey proposed some mechanisms for ferromagnetism based on lattice defect-related ferromagnetism which supposes that the defects in undoped semiconductors or insulator materials create states in the gap which are sufficiently numerous to form an impurity band.[29,197] If the density of states of these defects is sufficiently large, spontaneous spin splitting may occur which induces the room temperature ferromagnetism. Another mechanism proposed by Coey is that the defect states themselves can induce magnetic moments associated with molecular orbitals localized in the vicinity of the defects.[197] These states then form the impurity band which needed to mediate a long-range ferromagnetic interaction between them. The assumptions about the origin of the ferromagnetic behavior in such materials have mostly focused on:[194]

(i) Spin polarized anion p-orbital holes resulting from cation vacancies, under-coordinated surface anions, and impurity p states as in C and N doping.

(ii) Anion vacancies carrying unpaired electrons, such as F+ centers (singly occupied oxygen vacancies) in ZnO,

For more great information about the proposed mechanisms of room temperature ferromagnetism, the author suggests reading these published studies.[198–202]

SUMMARY AND FUTURE

Spintronics based magnetic semiconductor oxides is one of the most promising areas in recent years. In this work, we have introduced a systematic discussion on two interesting results: room temperature ferromagnetism in undoped semiconductor oxides and nonmagnetic dopants can induce ferromagnetism in oxides. Because of the large number of publications in recent years we can predict that some important investigations on this topic have been missed in the current study. Until now, semiconductor oxides possessing stable and robust room temperature ferromagnetism and a clear ferro-ordering mechanism with high control of spin polarization is not yet realized. In the future, the scientific strategies can include the search for novel

Table IV. Room temperature ferromagnetism induced by nonmagnetic nonmetal dopants in metal oxide semiconductors

Materials	Dopant	Preparation method	Saturation magnetization or magnetic moment (best sample)	References
TiO_2	C	Ion beam irradiation	7.5×10^{-2} emu/g	183
ZnO	C	Nanobeam-2 installation	1.1 emu/g	184
ZnO	C	Pulsed laser deposition	$\sim$ 7 emu/ cm^3	185
ZnO	C/N	Pulsed laser deposition	7.5 emu/ cm^3	186
ZnO	C	Mild C^+ ion implantation	2.7 emu/ cm^3	187
ZnO	C	Pulsed laser deposition	0.24 μB/C	188
ZnO	C	Ion-beam irradiation	–	189
TiO_2	N	Commercial rutile TiO_2 single crystals	–	190
CrO_2	N	Chemical vapor deposition	1.22 μB per f.u.	191
ZnO	N	rf magnetron sputtering	$\sim$ 4.8 emu/ cm^3	192
ZnO	B	Template-free solvothermal	0.0178 mA·m^2 ·kg^{-1}	193

materials and mechanisms or greatly improving the current ferromagnetic-semiconducting materials, such as the promising ZnO. These strategies can include working on different directions:

(i): Innovation of novel room temperature magnetic semiconductors with strong ferromagnetism and perfect spin current control through using new materials including two-dimensional materials, organic semiconductors and inorganic-organic hybrid perovskites.

(ii): Discovery of new mechanisms with good understanding and controlling of magnetic ordering to design the desired valuable properties.

(iii) Technical strategies include developing of new synthesis methods to obtained different morphologies, nanosize controlling, atomic-scale design and using of new combination of co-dopants or tri-dopant blends.

(v): Thin film preparation under different atmospheres and temperature to control in the type and concentration of defects.

In the final, we felling that with the continuous scientific researches, we are confident of reaching impressive results in the future.

CONFLICT OF INTEREST

The authors declare that they have no conflict of interest.

REFERENCES

1. D.D. Awschalom, D. Loss, and N. Samarth, *Semiconductor spintronics and quantum computation* Springer, Verlag Berlin Heidelberg, 2002.
2. J. Orton, semiconductors and the information revolution. (Elsevier, 2009).
3. X. Lin, W. Yang, K.L. Wang, and W. Zhao, X. Lin, W. Yang, K.L. Wang, and W. Zhao, *Nature Electronics*, 2019, 2, p 274.
4. V. K. Joshi, Engineering Science and Technology, an International Journal 19, 1503 (2016).
5. S. L. Harris and D. M. Harris, in Digital Design and Computer Architecture, ed. by M. Kaufmann (Elsevier, 2016), p. 238.
6. Y. Zhang, W. Zhao, J.-O. Klein, W. Kang, D. Querlioz, Y. Zhang, D. Ravelosona and C. Chappert, in IEEE conferences Xplore (2014), p. 1. https://doi.org/10.7873/DATE.2014.316.
7. S.E. Thompson, and S. Parthasarathy, S.E. Thompson, and S. Parthasarathy, *Mater. Today*, 2006, 9, p 20.
8. M. Johnson, in Magnetoelectronics, ed. by M. Johnson (Elsevier, 2004) p. 1.
9. T.B. Hook, T.B. Hook, *Joule*, 2018, 2, p 1.
10. T. Hiramoto, T. Hiramoto, *Nature Electronics*, 2019, 2, p 557.
11. L.B. Chandrasekar, K. Gnanasekar, and M. Karunakaran, *Superlattices Microstruct.*, 2019, 136, p 106322.
12. W. Liu, P.K.J. Wong, and Y. Xu, W. Liu, P.K.J. Wong, and Y. Xu, *Prog. Mater Sci.*, 2019, 99, p 27.
13. T. Ryhänen, M. A. Uusitalo, O. Ikkala and A. Kärkkäinen, Nanotechnologies for future mobile devices, (Cambridge University Press, 2010).
14. T. Yu-Feng, H. Shu-Jun, Y. Shi-Shen, and M. Liang-Mo, *Chin. Phys. B*, 2013, 22, p 088505.
15. Y.B. Xu, E. Ahmad, J.S. Claydon, Y.X. Lu, S.S.A. Hassan, I.G. Will, and B. Cantor, *J. Magn. Magn. Mater.*, 2006, 304, p 69.
16. T. Dietl, T. Dietl, *Nat. Mater.*, 2010, 9, p 965.
17. J. A. Gaj, in Comprehensive Semiconductor Science and Technology, ed. by P. Bhattacharya, H. Kamimura and R. Fornari (Elsevier, 2011), p. 95.
18. A. Gupta, R. Zhang, P. Kumar, V. Kumar, and A. Kumar, *Magnetochemistry*, 2020, 6, p 15.
19. T. Dietl, H. Ohno, F. Matsukura, J. Cibert, and D. Ferrand, *Science*, 2000, 287, p 1019.
20. Y. Matsumoto, M. Murakami, T. Shono, T. Hasegawa, T. Fukumura, M. Kawasaki, P. Ahmet, T. Chikyow, S. Koshihara, and H. Koinuma, *Science*, 2001, 291, p 854.
21. K. Ueda, H. Tabata, and T. Kawai, K, *Appl. Phys. Lett.*, 2001, 79, p 988.
22. H. Saeki, H. Tabata, and T. Kawai, *Solid State Commun.*, 2001, 120, p 439.
23. S.-J. Han, J.W. Song, C.-H. Yang, S.H. Park, J.-H. Park, and Y.H. Jeonga, *Appl. Phys. Lett.*, 2002, 81, p 4212.
24. Y.M. Cho, and W.K. Choo, *Appl. Phys. Lett.*, 2002, 80, p 3358.
25. W. Prellier, A. Fouchet, and B. Mercey, *J. Phys.: Condens. Matter*, 2003, 15, p R1583.
26. S.A. Chambers, T.C. Droubay, C.M. Wang, K.M. Rosso, S.M. Heald, D.A. Schwartz, K.R. Kittilstved, and D.R. Gamelin, *Mater. Today*, 2006, 9, p 28.
27. Y. Li, J. Li, Z. Yu, W. Li, M. Zhu, H. Jin, Y. Liu, Y. Li, and K. Skotnicova, *Ceram. Int.*, 2019, 45, p 19583.
28. A. Sundaresan, R. Bhargavi, N. Rangarajan, U. Siddesh, and C.N.R. Rao, *Physical Review B*, 2006, 74, p 161306(R).
29. J.M.D. Coey, J.M.D. Coey, *Nat. Mater.*, 2019, 18, p 652.
30. R.J. Green, D.W. Boukhvalov, E.Z. Kurmaev, L.D. Finkelstein, H.W. Ho, K.B. Ruan, L. Wang, and A. Moewes, *Phys. Rev. B*, 2012, 86, p 115212.
31. S.M. Yakout, H.A. Mousa, H.T. Handal, and W. Sharmoukh, *J. Solid State Chem.*, 2020, 281, p 121028.
32. Y. Liu, C. Zeng, J. Zhong, J. Ding, Z.M. Wang, and Z. Liu, *Nano-Micro Lett.*, 2020, 12, p 93.
33. H. Li, S. Ruan, and Y.-J. Zeng, *Adv. Mater.*, 2019, 31, p 1900065.
34. E. C. Ahn, npj 2D Materials and Applications **4**, 17 (2020).
35. M. Venkatesan, C.B. Fitzgerald, and J.M.D. Coey, *Nature*, 2004, 430, p 630.
36. D.B. Buchholz, and R.P.H. Chang, *Appl. Phys. Lett.*, 2005, 87, p 082504.
37. J.M.D. Coey, M. Venkatesan, P. Stamenov, C.B. Fitzgerald, and L.S. Dorneles, *Physical Review B*, 2005, 72, p 024450.
38. N.H. Hong, J. Sakai, N. Poirot, and V. Brizé, *Physical Review B*, 2006, 73, p 132404.
39. H.-M. Xiao, L.-P. Zhu, X.-M. Liu, and S.-Y. Fu, *Solid State Commun.*, 2007, 141, p 431.
40. A.K. Rumaiz, B. Ali, A. Ceylan, M. Boggs, T. Beebe, and S.I. Shah, *Solid State Commun.*, 2007, 144, p 334.
41. S.D. Yoon, Y. Chen, A. Yang, T.L. Goodrich, X. Zuo, K. Ziemer, C. Vittoria, and V.G. Harris, *J. Magn. Magn. Mater.*, 2007, 309, p 171.
42. D. Sanyal, M. Chakrabarti, T.K. Roy, and A. Chakrabarti, *Phys. Lett. A*, 2007, 371, p 482.
43. C. Sudakar, P. Kharel, R. Suryanarayanan, J.S. Thakur, V.M. Naik, R. Naik, and G. Lawes, *J. Magn. Magn. Mater.*, 2008, 320, p L31.
44. A. Hassini, J. Sakai, J.S. Lopez, and N.H. Hong, *Phys. Lett. A*, 2008, 372, p 3299.
45. A. Sundaresan, and C.N.R. Rao, *Nano Today*, 2009, 4, p 96.
46. Z. Li, W. Zhong, X. Li, H. Zeng, G. Wang, W. Wang, Z. Yang, and Y. Zhang, *J. Mater. Chem. C*, 2013, 1, p 6807.
47. Q. Xu, D. Gao, J. Zhang, Z. Yang, Z. Zhang, J. Rao, and D. Xue, *Appl. Phys. A*, 2014, 116, p 1293.
48. D. Gao, J. Li, Z. Li, Z. Zhang, J. Zhang, H. Shi, and D. Xue, *J. Phys. Chem. C*, 2010, 114, p 11703.
49. Z. Zhu, D. Gao, G. Yang, J. Zhang, J. Zhang, Z. Shi, F. Xu, H. Gao, and D. Xue, *EPL*, 2012, 97, p 17005.
50. J. Zhang, D. Gao, M. Si, Z. Zhu, G. Yang, Z. Shia, and D. Xue, *J. Mater. Chem. C*, 2013, 1, p 6216.

51. D. Gao, Z. Zhang, Y. Li, B. Xia, S. Shi, and D. Xue, *Chem. Commun.*, 2015, 51, p 1151.
52. C. Sudakar, K. Padmanabhan, R. Naik, G. Lawes, B.J. Kirby, S. Kumar, and V.M. Naik, *Appl. Phys. Lett.*, 2008, 93, p 042502.
53. W. Wang, L. Xu, R. Zhang, J. Xu, F. Xian, J. Su, and F. Yang, *Chem. Phys. Lett.*, 2019, 721, p 57.
54. Q. Xu, Z. Wen, L. Xu, J. Gao, D. Wu, K. Shen, T. Qiu, S. Tang, and M. Xu, *Phys. B*, 2011, 406, p 19.
55. X. Bie, C. Wang, H. Ehrenberg, Y. Wei, G. Chen, X. Meng, G. Zou, and F. Du, *Solid State Sci.*, 2010, 12, p 1364.
56. H. Zhang, W. Li, G. Qin, H. Ruan, D. Wang, J. Wang, C. Kong, F. Wu, and L. Fang, *Solid State Commun.*, 2019, 292, p 36.
57. X. Hou, H. Liu, H. Sun, L. Liu, and X. Jia, *Mater. Sci. Eng., B*, 2015, 200, p 22.
58. A.K. Das, M. Kar, and A. Srinivasan, *Phys. B*, 2014, 448, p 112.
59. G. Jayalakshmi, N. Gopalakrishnan, and T. Balasubramanian, *J. Alloy. Compd.*, 2013, 551, p 667.
60. S. Kumar, Y.J. Kim, B.H. Koo, S. Gautam, K.H. Chae, R. Kumar, and C.G. Lee, *Mater. Lett.*, 2009, 63, p 194.
61. S.-W. Kim, S. Lee, A.N.S. Saqib, Y.H. Lee, and M.-H. Jung, *Curr. Appl. Phys.*, 2017, 17, p 181.
62. B. Kisan, and P. Alagarsamy, *Phys. B*, 2014, 448, p 115.
63. B.B. Straumal, A.A. Mazilkin, S.G. Protasova, A.A. Myatiev, P.B. Straumal, E. Goering, and B. Baretzky, *Thin Solid Films*, 2011, 520, p 1192.
64. C. Zhao, Y. Huang, and J.T. Abiade, *Mater. Lett.*, 2012, 85, p 164.
65. H. Liu, G. P. Li, D. J. E, N. N. Xu, Q. L. Lin, X. D. Gao and C. L. Wang, Journal of Superconductivity and Novel Magnetism 33, 1535 (2020).
66. X. Liu, J. Bu, X. Ren, B. Cheng, J. Xie, L. Chen, C. Gao, L. Liu, H. Zhang, G. Zhou, H. Qin, and J. Hu, *J. Magn. Magn. Mater.*, 2019, 475, p 368.
67. J. Li, G. Bai, Y. Jiang, Y. Du, C. Wu, and M. Yan, *J. Magn. Magn. Mater.*, 2017, 426, p 545.
68. K. Sakthiraj, M. Hema, and K.B. Kumar, *Appl. Surf. Sci.*, 2017, 420, p 145.
69. V.S. Jahnavi, S.K. Tripathy, and A.V.N.R. Rao, *Phys. B*, 2019, 565, p 61.
70. T. Wu, H. Sun, X. Hou, L. Liu, H. Zhang, and J. Zhang, *Microporous Mesoporous Mater.*, 2014, 190, p 63.
71. A.S. Bolokang, F.R. Cummings, B.P. Dhonge, H.M.I. Abdallah, T. Moyo, H.C. Swart, C.J. Arendse, T.F.G. Muller, and D.E. Motaung, *Appl. Surf. Sci.*, 2015, 331, p 362.
72. D. Wang, Y. Qiu, W. Li, H. Zhang, G. Qin, H. Ruan, L. Ye, C. Kong, and L. Fang, *J. Mater. Sci.: Mater. Electron.*, 2019, 30, p 11086.
73. X. Zhang, W. Zhang, X. Zhang, X. Xu, F. Meng, and C.C. Tang, X. Zhang, W. Zhang, X. Zhang, X. Xu, F. Meng, and C.C. Tang, *Advances in Condensed Matter Physics*, 2014, 2014, p 806327.
74. D. Gao, Z. Zhang, J. Fu, Y. Xu, J. Qi, and D. Xue, *J. Appl. Phys.*, 2009, 105, p 113928.
75. D. Mishra, C.S. Rout, M. Mishra, and A.K. Pattanaik, *Integrated Ferroelectrics*, 2017, 184, p 124.
76. S. Phokha, E. Swatsitang, and S. Maensiri, *Electron. Mater. Lett.*, 2015, 11, p 1012.
77. D. Gao, G. Yang, J. Li, J. Zhang, J. Zhang, and D. Xue, *J. Phys. Chem. C*, 2010, 114, p 18347.
78. J.A. Souza, D. Criado, A. Zuniga, V.N. Miranda, F.E.N. Ramirez, S.H. Masunaga, and R.F. Jardim, *J. Appl. Phys.*, 2013, 114, p 173907.
79. D. Gao, J. Zhang, J. Zhu, J. Qi, Z. Zhang, W. Sui, H. Shi, and D. Xue, *Nanoscale Res Lett*, 2010, 5, p 769.
80. S. Shi, D. Gao, B. Xia, and D. Xue, *J. Phys. D: Appl. Phys.*, 2016, 49, p 055003.
81. S. Duhalde, M. F. Vignolo, F. Golmar, C. Chiliotte, C. E. Rodríguez Torres, L. A. Errico, A. F. Cabrera, M. Rentería, F. H. Sánchez and M. Weissmann, *Physical Review* B 72, 161313(R) (2005).
82. T.S. Herng, S.P. Lau, S.F. Yu, H.Y. Yang, X.H. Ji, J.S. Chen, N. Yasui, and H. Inaba, *J. Appl. Phys.*, 2006, 99, p 086101.
83. D.L. Hou, X.J. Ye, X.Y. Zhao, H.J. Meng, H.J. Zhou, X.L. Li, and C.M. Zhen, *J. Appl. Phys.*, 2007, 102, p 033905.
84. D. Gao, Y. Xu, Z. Zhang, H. Gao, and D. Xuea, *J. Appl. Phys.*, 2009, 105, p 063903.
85. S.K. Alla, P. Kollu, R.K. Mandala, and N.K. Prasad, *Ceram. Int.*, 2018, 44, p 7221.
86. Y. Chen, X. Xu, X. Li, and G. Zhang, *Appl. Surf. Sci.*, 2020, 506, p 144905.
87. M. Venkatesan, C.B. Fitzgerald, J.G. Lunney, and J.M.D. Coey, *Phys. Rev. Lett.*, 2004, 93, p 177206.
88. K. Sakthiraj, and K. Balachandrakumar, *J. Magn. Magn. Mater.*, 2015, 395, p 205.
89. R.N. Bhowmik, P. Mitra, R.J. Choudhury, and V.R. Reddy, *Appl. Surf. Sci.*, 2020, 501, p 144224.
90. Z.D. Dohčević-Mitrović, N. Paunović, B. Matović, P. Osiceanu, R. Scurtu, S. Aškrabić, and M. Radović, *Ceram. Int.*, 2015, 41, p 6970.
91. W. Lee, S.-Y. Chen, Y.-S. Chen, C.-L. Dong, H.-J. Lin, C.-T. Chen, and A. Gloter, *J. Phys. Chem. C*, 2014, 118, p 26359.
92. X. Ma, P. Lu, and P. Wu, *Ceram. Int.*, 2018, 44, p 15989.
93. G. Murtaza, R. Ahmad, M. S. Rashid, M. Hassan, A. Hussnain, M. A. Khan, M. E. ul Haq, M. A. Shafique and S. Riaz, Current Applied Physics 14, 176 (2014).
94. X. Liu, J. Iqbal, Z. Wu, B. He, and R. Yu, *J. Phys. Chem. C*, 2010, 114, p 4790.
95. F. Paraguay-Delgado, F.C. Vasquez, J.T. Holguín-Momaca, C.R. Santillán-Rodríguez, J.A. Matutes-Aquino, and S.F. Olive-Méndez, *J. Magn. Magn. Mater.*, 2019, 476, p 183.
96. M. Debbichi, M. Souissi, A. Fouzri, G. Schmerber, M. Said, and M. Alouani, *J. Alloy. Compd.*, 2014, 598, p 120.
97. M. Souissi, A. Fouzri, and G. Schmerber, *Solid State Commun.*, 2015, 218, p 40.
98. S. Ramya, R. Gobi, N. Shanmugam, G. Viruthagiri, and N. Kannadasan, *J Mater Sci: Mater Electron*, 2016, 27, p 40.
99. Q. Xu, Z.-J. Wang, Z.-J. Chang, J.-J. Liu, Y.-X. Ren, and H.-Y. Sun, *Chem. Phys. Lett.*, 2016, 666, p 28.
100. N. Ali, A.R. Vijaya, Z.A. Khan, K. Tarafder, A. Kumar, M.K. Wadhwa, B. Singh, and S. Ghosh, *Scientific Reports*, 2019, 9, p 20039.
101. Y. Yang, W. Zhou, Y. Liang, L. Liu, and P. Wu, *J. Cryst. Growth*, 2015, 430, p 75.
102. X. Lu, Y. Liu, X. Si, Y. Shen, W. Yu, W. Wang, X. Luo, and T. Zhou, *Opt. Mater.*, 2016, 62, p 335.
103. K.W. Liu, M. Sakurai, and M. Aono, *J. Appl. Phys.*, 2010, 108, p 043516.
104. S. Singh, N. Jahan, A. Khanna, G. Singh, Lotey and N. K. Verma, Chalcogenide Letters 9, 73 (2012).
105. J. Kazmi, P.C. Ooi, B.T. Goh, M.K. Lee, M.F.M.R. Wee, S.S.A. Karim, S.R.A. Razad, and M.A. Mohamed, *RSC Adv.*, 2020, 10, p 23297.
106. J. Lee, G.S. Nagarajan, Y. Shon, Y. Kwon, T.W. Kang, D.Y. Kim, H. Kim, H. Im, C.-S. Park, and E.K. Kim, *AIP Adv.*, 2017, 7, p 085114.
107. T. Li, H. Fan, J. Yi, T.S. Herng, Y. Ma, X. Huang, J. Xue, and J. Ding, *J. Mater. Chem.*, 2010, 20, p 5756.
108. C.G. Jin, T. Yu, Y. Yang, Z.F. Wu, L.J. Zhuge, X.M. Wu, and Z.C. Feng, *Mater. Chem. Phys.*, 2013, 139, p 506.
109. W. Wan, J. Huang, L. Zhu, L. Hu, Z. Wen, L. Sun, and Z. Ye, *CrystEngComm*, 2013, 15, p 7887.
110. B. Babu, T. Aswani, G. Thirumala Rao, R. Joyce Stella, B. Jayaraja and R. V. S. S. N. Ravikumar, Journal of Magnetism and Magnetic Materials 355, 76 (2014).
111. D. Li, D.K. Li, H.Z. Wu, F. Liang, W. Xie, C.W. Zou, and L.X. Shao, *J. Alloy. Compd.*, 2014, 591, p 80.
112. L. Zhang, L. Zhu, L. Hu, Y. Zeng, and Z. Ye, L. Zhang, *J. Alloy. Compd.*, 2016, 684, p 132.
113. M. Zhu, Z. Zhang, M. Zhong, M. Tariq, Y. Li, W. Li, H. Jin, K. Skotnicova, and Y. Li, *Ceram. Int.*, 2017, 43, p 3166.
114. Y. Wang, J. Hao, G. Gong, R. Chen, and Y. Su, *Phys. B*, 2019, 564, p 22.

115. P. Chetri, and A. Choudhury, *J. Alloy. Compd.*, 2015, 627, p 261.
116. A. Johari, S. Srivastav, M. Sharm, and M.C. Bhatnagar, *J. Magn. Magn. Mater.*, 2014, 362, p 1.
117. B. Choudhury, A. Choudhury, and D. Borah, *J. Alloy. Compd.*, 2015, 646, p 692.
118. Z. Zhou, H. Wang, Z. Zou, M. Du, J. Guo, and Z. Yang, *Mater. Res. Bull.*, 2017, 86, p 287.
119. F.A. Al-Agel, E. Al-Arfaj, A.A. Al-Ghamdi, B.D. Stein, Y. Losovyj, L.M. Bronstein, F.S. Shokr, and W.E. Mahmoud, *Ceram. Int.*, 2015, 41, p 1115.
120. D. Li, D. Li, and C. Zou, *J. Alloy. Compd.*, 2015, 650, p 912.
121. R.O. Ijeh, A.C. Nwanya, A.C. Nkele, I.G. Madiba, Z. Khumalo, A.K.H. Bashir, R.U. Osuji, M. Maaza, and F.I. Ezema, *Physica E*, 2019, 113, p 233.
122. E.T. Selvi, and S.M. Sundar, *Appl. Phys. A*, 2017, 123, p 383.
123. J. Li, Y. Li, S. Li, M. Zhu, J. Zhang, Y. Li, Y. He, and W. Li, *Ceram. Int.*, 2020, 46, p 18639.
124. J. Wang, W. Zhou, and P. Wu, *J Nanopart Res*, 2014, 16, p 2573.
125. T. Yingsamphancharoen, P. Nakarungsee, T.S. Herng, J. Ding, I.M. Tang, and S. Thongmee, *J. Magn. Magn. Mater.*, 2016, 419, p 274.
126. H.K. Mallick, Y. Zhang, J. Pradhan, M.P.K. Sahoo, and A.K. Pattanaik, *J. Alloy. Compd.*, 2021, 854, p 156067.
127. A.S. Ganeshraja, S. Thirumurugan, K. Rajkumar, K. Zhu, Y. Wang, K. Anbalagan, and J. Wang, *RSC Adv.*, 2016, 6, p 409.
128. M.H. Farooq, R. Hussain, M.Z. Iqbal, M.W. Shah, U.A. Rana, and S.U.-D. Khan, *J. Nanosci. Nanotechnol.*, 2016, 16, p 898.
129. K.C. Kumar, S. Kaleemulla, C. Krishnamoorthi, N.M. Rao, and G.V. Rao, *J. Supercond. Novel Magn.*, 2019, 32, p 1725.
130. K. Sedeek, E. Abdeltwab, H. Hantour, and N. Makram, K. Sedeek, E. Abdeltwab, H. Hantour, and N. Makram, *J. Supercond. Novel Magn.*, 2020, 33, p 445.
131. S. Zhou, L. Liu, S. Lou, Y. Wang, X. Chen, H. Yuan, Y. Hao, R. Yuan, and N. Li, *Appl Phys A*, 2011, 102, p 367.
132. S. Chawla, K. Jayanthi, and R.K. Kotnala, *Physical Review B*, 2009, 79, p 125204.
133. J.B. Yi, C.C. Lim, G.Z. Xing, H.M. Fan, L.H. Van, S.L. Huang, K.S. Yang, X.L. Huang, X.B. Qin, B.Y. Wang, T. Wu, L. Wang, H.T. Zhang, X.Y. Gao, T. Liu, A.T.S. Wee, Y.P. Feng, and J. Ding, *Phys. Rev. Lett.*, 2010, 104, p 137201.
134. C. Y. Kung, C. C. Lin, S. L. Young, Lance Horng, Y. T. Shih, M. C. Kao, H. Z. Chen, H. H. Lin, J. H. Lin, S. J. Wang and J. M. Li, Thin Solid Films 529, 181 (2013).
135. H. Cao, P. Xing, W. Zhou, D. Yao, and P. Wu, *J. Magn. Magn. Mater.*, 2018, 451, p 609.
136. B.K. Pandey, A.K. Shahi, J. Shah, R.K. Kotnala, and R. Gopal, *J. Alloy. Compd.*, 2020, 823, p 153710.
137. J. Wang, D. Zhou, Y. Li, and P. Wu, *Vacuum*, 2017, 141, p 62.
138. W. Zhou, X. Tang, P. Xing, W. Liu, and P. Wu, *Phys. Lett. A*, 2012, 376, p 203.
139. Y. Huang, W. Zhou, and P. Wu, *Solid State Commun.*, 2014, 183, p 31.
140. U.K. Panigrahi, V. Sathe, P.D. Babu, A. Mitra, and P. Mallick, *Nano Express*, 2020, 1, p 020009.
141. P. Wu, B. Zhou, and W. Zhou, *Appl. Phys. Lett.*, 2012, 100, p 182405.
142. Z. Quan, X. Liu, Y. Qi, Z. Song, S. Qi, G. Zhou, and X. Xu, *Appl. Surf. Sci.*, 2017, 399, p 751.
143. M.C. Dimri, H. Khanduri, H. Kooskora, M. Kodu, R. Jaaniso, I. Heinmaa, A. Mere, J. Krustok, and R. Stern, *J. Phys. D: Appl. Phys.*, 2012, 45, p 475003.
144. N. Rajamanickam, S.S. Kanamni, S. Rajashabala, and K. Ramachandran, *Mater. Lett.*, 2015, 161, p 520.
145. N. Wang, W. Zhou, Y. Liang, W. Cui, and P. Wu, *J Mater Sci: Mater Electron*, 2015, 26, p 7751.
146. J. Wang, W. Zhou, and P. Wu, *Appl. Surf. Sci.*, 2014, 314, p 188.
147. S. Akbar, S.K. Hasanain, O. Ivashenko, M.V. Dutka, N.Z. Ali, G.R. Blake, JTh.M. De Hosson, and P. Rudolf, *RSC Adv.*, 2020, 10, p 26342.
148. S.U. Awan, S.K. Hasanain, D.H. Anjum, M.S. Awan, and S.A. Shah, S.U. Awan, S.K. Hasanain, D.H. Anjum, M.S. Awan, and S.A. Shah, *J. Appl. Phys.*, 2014, 116, p 164109.
149. S.U. Awan, S.K. Hasanain, M.F. Bertino, and G.H. Jaffari, *J. Appl. Phys.*, 2012, 112, p 103924.
150. R. Vettumperumal, S. Kalyanaraman, B. Santoshkumar, and R. Thangavel, *Mater. Res. Bull.*, 2014, 50, p 7.
151. S. Ghosh, G.G. Khan, K. Mandal, S. Thap, and P.M.G. Nambissan, *J. Alloy. Compd.*, 2014, 590, p 396.
152. S. Tanyawong, I. Tang, T.S. Herng, and S. Thongmee, *J. Supercond. Novel Magn.*, 2020, 33, p 285.
153. M.H. Farooq, H.L. Yang, M.Y. Rafique, and M.Z. Iqbal, *Journal of Spintronics and Magnetic Nanomaterials*, 2012, 1, p 122.
154. R. Krithiga, S. Sankar, and V. Arunkumar, *J Supercond Nov Magn*, 2016, 29, p 245.
155. S. Ghosh, G.G. Khan, B. Das, and K. Mandal, *J. Appl. Phys.*, 2011, 109, p 123927.
156. W.U. Kai, X.U. Xiaoguang, Y. Hailing, Z. Jianli, M. Jun, and J. Yong, *Rare Met.*, 2012, 31, p 27.
157. J. Piao, L.-T. Tseng, K. Suzuki, and J. Yi, *Functional Materials Letters*, 2016, 9, p 1650039.
158. S. Ghosh, G.G. Khan, S. Varma, and K. Mandal, *Mater. Interfaces*, 2013, 5, p 2455.
159. Y. Wang, X. Luo, L.-T. Tseng, Z. Ao, T. Li, G. Xing, N. Bao, K. Suzukiis, J. Ding, S. Li, and J. Yi, *Chem. Mater.*, 2015, 27, p 1285.
160. A.H. Maru, H. Kamble, A. Kalarikkal, R. Shah, P.B. Bhanuse, and N. Pradhan, *International Journal of Chemical and Physical Sciences*, 2015, 5, p 44.
161. T. Ali, A. Ahmed, M.N. Siddique, and P. Tripathi, *Optik*, 2020, 223, p 165340.
162. K. Yang, Y. Dai, B. Huang, and M.-H. Whangbo, *Appl. Phys. Lett.*, 2008, 93, p 132507.
163. X.J. Ye, W. Zhong, M.H. Xu, X.S. Qi, C.T. Au, and Y.W. Du, *Phys. Lett. A*, 2009, 373, p 3684.
164. A. Ablat, R. Wu, M. Mamat, Y. Ghupur, A. Aimidula, M.A. Bake, T. Gholam, J. Wang, H. Qian, R. Wu, and K. Ibrahim, *Solid State Commun.*, 2016, 243, p 7.
165. X.J. Ye, C.S. Liu, W. Zhong, H.A. Song, C.T. Au, and Y.W. Du, *Phys. Lett. A*, 2010, 374, p 496.
166. S. Akbar, S.K. Hasanain, M. Abbas, S. Ozcan, B. Ali, and S.I. Shah, *Solid State Commun.*, 2011, 151, p 17.
167. C.S. Wei, S.P. Lau, M. Tanemura, M. Subramanian, and Y. Akaike, *Appl. Surf. Sci.*, 2012, 258, p 5486.
168. N.D. Dung, C.T. Son, P.V. Loc, N.H. Cuong, P.T. Kien, P.T. Huy, and N.N. Ha, *J. Alloy. Compd.*, 2016, 668, p 87.
169. J.J. Beltrán, C.A. Barrero, and A. Punnoose, *Phys. Chem. Chem. Phys.*, 2019, 21, p 8808.
170. K.B. Ruan, H.W. Ho, R.A. Khan, P. Ren, W.D. Song, A.C.H. Huan, and L. Wang, *Solid State Commun.*, 2010, 150, p 2158.
171. R.A. Khan, A.S. Bhatti, and R. Kaibin, *J. Magn. Magn. Mater.*, 2011, 323, p 2841.
172. L. Shen, Y. An, D. Cao, Z. Wu, and J. Liu, *J. Phys. Chem. C*, 2017, 121, p 26499.
173. N.N. Bao, H.M. Fan, J. Ding, and J.B. Yi, *J. Appl. Phys.*, 2011, 109, p 07C302.
174. C. Gómez-Polo, S. Larumbe, and J.M. Pastor, *J. Appl. Phys.*, 2013, 113, p 17B511.
175. A. Ablat, R. Wu, J. Jian, X. Jiang, M. Mamat, J. Li, and H. Ren, *Mater. Lett.*, 2014, 132, p 86.
176. C. Gómez-Polo, S. Larumbe, and M. Monge, *J. Alloy. Compd.*, 2014, 612, p 450.
177. C.-C. Wang, C.-M. Fu, and Y.-M. Hu, *Surf. Coat. Technol.*, 2013, 231, p 307.
178. C.-F. Yu, S.-J. Sun, H.-S. Hsu, and H. Chou, *Phys. Lett. A*, 2014, 378, p 1965.
179. B. Zhou, S. Dong, H. Zhao, Y. Liu, and P. Wu, *J. Magn. Magn. Mater.*, 2014, 362, p 14.

180. Q. Li, B. Ye, Y. Hao, J. Liu, J. Zhang, L. Zhang, W. Kong, H. Weng, and B. Ye, *Chem. Phys. Lett.*, 2013, 556, p 237.
181. S. Yılmaza, J. Nisar, Y. Atasoy, E. McGlynn, R. Ahuja, M. Parlak, and E. Bacaksız, *Ceram. Int.*, 2013, 39, p 4609.
182. X.G. Xu, H.L. Yang, Y. Wu, D.L. Zhang, S.Z. Wu, J. Miao, Y. Jiang, X.B. Qin, X.Z. Cao, and B.Y., *Appl. Phys. Lett.*, 2010, 97, p 232502.
183. H. Luitel, P. Chettri, A. Tiwari, and D. Sanyal, *Mater. Res. Bull.*, 2019, 110, p 13.
184. V. G. Il'ves and S. Y. Sokovnin, Journal of Magnetism and Magnetic Materials 441, 131 (2017).
185. H. Pan, J.B. Yi, L. Shen, R.Q. Wu, J.H. Yang, J.Y. Lin, Y.P. Feng, J. Ding, L.H. Van, and J.H. Yin, *Phys. Rev. Lett.*, 2007, 99, p 127201.
186. J.B. Yi, L. Shen, H. Pan, L.H. Van, S. Thongmee, J.F. Hu, Y.W. Ma, J. Ding, and Y.P. Feng, *J. Appl. Phys.*, 2009, 105, p 07C513.
187. Y.F. Wang, Y.C. Shao, S.H. Hsieh, Y.K. Chang, P.H. Yeh, H.C. Hsueh, J.W. Chiou, H.T. Wang, S.C. Ray, H.M. Tsai, C.W. Pao, C.H. Chen, H.J. Lin, J.F. Lee, C.T. Wu, J.J. Wu, Y.M. Chang, K. Asokan, K.H. Chae, T. Ohigashi, Y. Takagi, T. Yokoyama, N. Kosugi, and W.F. Pong, *Scientific Report*, 2018, 8, p 7758.
188. S. Zhou, Q. Xu, K. Potzger, G. Talut, R. Grötzsche, J. Fassbender, M. Vinnichenko, J. Grenzer, M. Helm, H. Hochmuth, M. Lorenz, M. Grundmann, and H. Schmidt, *Appl. Phys. Lett.*, 2008, 93, p 232507.
189. M. Subramanian, Y. Akaike, Y. Hayashi, M. Tanemura, H. Ebisu, and D.L.S. Ping, *Basic Solid State Physics*, 2012, 249, p 1254.
190. Q. Xiu-Bo, L. Dong-Xiang, L. Rui-Qin, Z. Peng, L. Yu-Xiao, and W. Bao-Yi, *Chinese Phys. B*, 2014, 23, p 067502.
191. Y. Li, Y. Liu, J. Shi, and R. Xiong, *Ceram. Int.*, 2018, 44, p 9664.
192. X. Nie, B. Zhang, J. Wang, L. Shi, Z. Di, and Q. Guo, *Mater. Lett.*, 2015, 161, p 355.
193. M.H. Farooq, X.-G. Xu, H.-L. Yang, C.-J. Ran, J. Miao, M.Z. Iqbal, and Y. Jiang, *Rare Met.*, 2013, 32, p 264.
194. Z. Zhang, U. Schwingenschlogl, and I.S. Roqan, *RSC Adv.*, 2014, 4, p 50759.
195. S.B. Singh, Y. Wang, Y. Shao, H. Lai, S. Hsieh, M.V. Limaye, C. Chuang, H. Hsueh, H. Wang, J. Chiou, H. Tsai, C. Pao, C. Chen, H. Lin, J. Lee, C. Wu, J. Wu, W. Pong, T. Ohigashi, N. Kosugi, J. Wang, J. Zhou, T. Regier, and T. Sham, *Nanoscale*, 2014, 6, p 9166.
196. L. Tien, and Y. Hsieh, *Mater. Res. Bull.*, 2014, 60, p 690.
197. J.M.D. Coey, *Solid State Sci.*, 2005, 7, p 660.
198. A. Pimachev, G. Rimal, R.D. Nielsen, J. Tang, and Y. Dahnovsky, *Phys. Chem. Chem. Phys.*, 2018, 20, p 29804.
199. S. Ninga, and Z. Zhang, *RSC Adv.*, 2015, 5, p 3636.
200. B. Santara, P.K. Giri, K. Imakita, and M. Fujii, *Nanoscale*, 2013, 5, p 5476.
201. S. Ghose, T. Rakshit, R. Ranganathanc, and D. Jana, *RSC Adv.*, 2015, 5, p 99766.
202. J.P. Singh, and K.H. Chae, *Condens. Matter*, 2017, 2, p 36.